Applied Catalysis B: Environmental 204 (2017) 440–455

Contents lists available at ScienceDirect

Applied Catalysis B: Environmental

journal homepage: www.elsevier.com/locate/apcatb

The visible-light-assisted thermocatalytic methanation of CO_2 over $Ru/TiO_{(2-x)}N_x$

Liuliu Lin, Ke Wang, Kai Yang, Xun Chen, Xianzhi Fu, Wenxin Dai*

State Key Laboratory of Photocatalysis on Energy and Environment, Research Institute of Photocatalysis, Fuzhou University, Fuzhou, 350002, PR China

ARTICLE INFO

Article history:
Received 16 September 2016
Received in revised form
20 November 2016
Accepted 24 November 2016
Available online 25 November 2016

Keywords:
CO_2 methanation
Visible-light-assisted effect
Electron transfer
CO_2 chemisorption
Nitrogen doped TiO_2

ABSTRACT

A $Ru/TiO_{(2-x)}N_x$ catalyst was prepared by impregnation-reduction method with loading Ru on the nitrogen doped TiO_2 support. This catalyst's performance for CO_2 methanation was evaluated under visible light irradiation ($435nm < \lambda < 465$ nm) or not, which was compared with that of Ru/TiO_2 catalyst. It was found that $Ru/TiO_{(2-x)}N_x$ exhibits a better catalytic activity than Ru/TiO_2 under visible light irradiation or not, and the promoted effect of visible light on the former is much more significant than that on the latter's. After comparing the results of chemisorption, temperature-programmed surface reaction, X-ray Photoelectron spectroscopy and photocurrent tests over $Ru/TiO_{(2-x)}N_x$ and Ru/TiO_2, it was found that the photo-assisted role on $Ru/TiO_{(2-x)}N_x$ mainly comes from two cases: (i) The $TiO_{(2-x)}N_x$ itself is prone to adsorb CO_2 and its activation into the CO species (as the intermediates of CO_2 methanation reaction), which visible light can further promote the process by forming much more significant oxygen vacancies over $TiO_{(2-x)}N_x$. (ii) The photo-generated electrons of $TiO_{(2-x)}N_x$ induced by visible light can transfer to the Ru nanoparticles, resulting in the increase in the surface electron density of Ru and then the promoted adsorption and activation of CO_2. For Ru/TiO_2, TiO_2 itself cannot transform the adsorbed CO_2 into the CO intermediates, which resulted in a lower thermo-catalytic activity for CO_2 methanation. Under visible light irradiation, the extrinsic excitation of TiO_2 cannot formation of new surface oxygen vacancies at TiO_2, but the photo-generated electrons can transfer from TiO_2 to Ru, which resulted in the increase of surface electron density and then the promoted adsorption and activation of CO_2 at Ru sites. Thus, a weaker photo-assisted effect for catalyzing CO_2 methanation can occur on Ru/TiO_2.

1. Introduction

Treatment of CO_2, so far, mainly was divided into two principal methods: the one of method is capturing and then storing CO_2 in geology, the other is converting CO_2 into useful chemicals or low carbon fuels [1], which is receiving considerable attention as a long-term alternative to the fossil fuels as well a mean to decrease CO_2 emission. CO_2 can be reduced into many useful products [2,3], such as urea and its derivatives, salicylic acid, formate or methanol etc [4–7]. Recently, it was focused on converting CO_2 into low carbon fuels by Fischer-Tropsch (F-T) synthesis, which of the products of CO_2 hydrogenation, such as methanol and dimethyl ether, were the desired fuels of micro-rotary internal combustion engine. However, the synthesis of hydrocarbon and alcohol by CO_2 hydrogenation usually occur under high pressure (5.0 MPa) [8]. Since the process of CO_2 methanation is much easier than the above processes the CO_2 methanation is also a process of effective CO_2 transformation [9].

Ru, Rh, Ni and Co catalysts have been reported to show the optimal thermo-catalytic activity for CO_2 methanation reaction [1]. Among them, the Ni catalysts have obtained extensive attentions in application research due to its high-efficient performance and low-cost price. However, the Ni catalysts are easily to form metal carbonyl compounds which leads to the passivation of active sites and the loss of its intrinsic active phase [10]. In addition, carbon deposit easily occurs on the surface of Ni active sites, result in inclining to sinter and the subsequent poison of catalysts [11,12]. Ru catalysts are considered to be the most activity catalyst at low reaction temperature in CO or CO_2 methanation [13–16], which show a very stable catalytic activity at a variable range of reaction temperatures [17]. In fact, a low reaction temperature is also more prone to the methanation process in thermodynamics ($CO_2 + 4H_2 \rightarrow CH_4 + 2H_2O$, $\triangle H^{\theta}_{298} = -165$ kJ/mol) according to its exothermic features, the great challenge for all catalysts is to obtain the thermodynamic equilibrium of this reaction in dynamics at a relative low temperature [18,19]. Therefore, how to further

* Corresponding author.
E-mail address: daiwenxin@fzu.edu.cn (W. Dai).

http://dx.doi.org/10.1016/j.apcatb.2016.11.054
0926-3373/

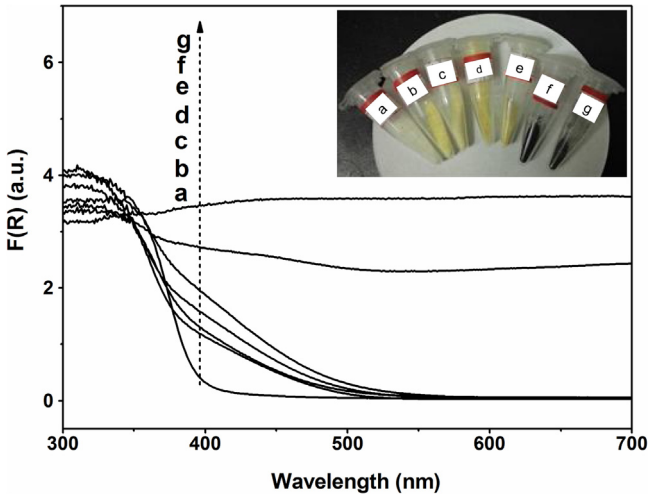

Fig. 1. UV–vis diffuse reflection spectra of different samples: (a) TiO_2, (b) $TiO_{1.98}N_{0.02}$, (c) $TiO_{1.91}N_{0.09}$, (d) $TiO_{1.85}N_{0.15}$, (e) $TiO_{1.82}N_{0.18}$, (f) Ru/TiO_2 and (g) $Ru/TiO_{1.85}N_{0.15}$.

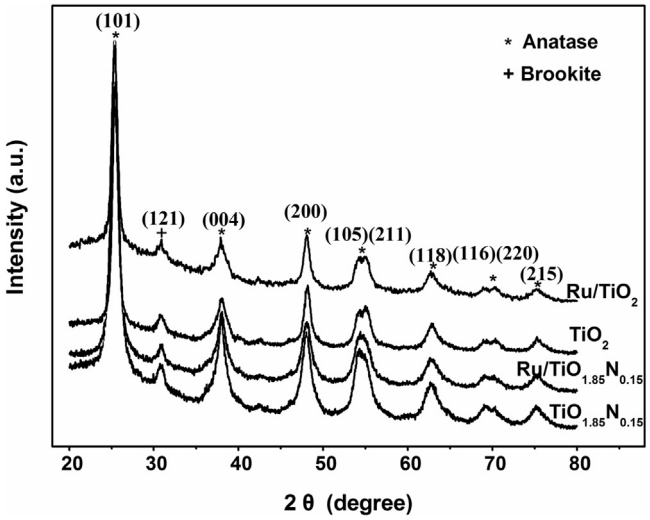

Fig. 2. XRD patterns of (a) Ru/TiO_2 (b) TiO_2 (c) $Ru/TiO_{1.85}N_{0.15}$ (d) $TiO_{1.85}N_{0.15}$ samples.

improve its catalytic activity at low temperature is still a great challenge for CO_2 methanation.

Most people generally agreed that the thermo-catalytic methanation of CO_2 proceeds along the following two steps: First CO_2 is converted into CO, and last CO is hydrogenated to CH_4 following the way of CO methanation [20–23]. William et al. [24] has analyzed the CO_2 methanation over Rh catalysts and found that the CO_2 methanation process begins with splitting CO_2 into an adsorbed CO and adsorbed O species, indicating that the factors being beneficial to the CO methanation process maybe also benefit to the proceeding of CO_2 methanation. For CO methanation process, it is mainly dependent on the adsorption and activation of CO over the metal active site [25–28]. Moreover, the high electron density of metal nanoparticles can promote the adsorption and activation of CO [29–31]. According to this viewpoint, the reducing support, such as TiO_2, can promote the CO methanation due to donating electron to metal nanoparticles by the interaction between support and metal nanoparticles [32]. Our group have also found that the ultravoilet (UV) light can promote the CO methanation over Ru/TiO_2, which can be attributed to the enhanced adsorption of CO and its activation at Ru nanoparticle surface due to the increase in electron density of Ru nanoparticles, resulted from the photo-generated electrons from TiO_2 to the adjacent Ru nanoparticles [33]. Similarly, the promoted effect induced by the interaction between the reducing support and active metals maybe also occurs on the CO_2 methanation reaction due to its including CO methanation process. E.g., the electrons transfer from CeO_2-SiO_2 support to Ni surface can benefit to the CO_2 methanation over Ni/CeO_2-SiO_2 [34]. Considering that the photo-excitation of semi-conductor can generate electrons, we think that introducing light into the semi-conductor supported metal catalysts maybe an approach to promote the CO_2 methanation in a low temperature.

Titanium dioxides, as a typical photo-excitation carrier, have been widely applied in many areas, such as solar energy conversion process and environment photo-catalytic purification in past decades [35]. However, TiO_2 is usually intrinsically excitated by UV light due to its wide band gap [36], resulting in the restrictions of TiO_2 photocatalysts in many cases. In order to broaden its light response region, TiO_2 was usually modified by doping other elements or combing with other semi-conducting oxides. E. g., a, nitrogen doped TiO_2 can be excited by the visible light [35–38].

Based on the above reports, in this work we designed a new approach to enhance the catalytic activity of Ru-based catalyst for CO_2 methanation at low temperature, i.e., loading Ru nanoparticles on the nitrogen-doped TiO_2 carrier and then introducing visible light into the reaction system of CO_2 methanation. It was expected that the visible-light-induced electrons of the nitrogen-doped TiO_2 can transfer to the surface of Ru nanoparticles, which promotes the adsorption of CO_2 and its activation at Ru surface and then CO_2 methanation. Fortunately, visible light did enhance the catalytic activity of the nitrogen-doped TiO_2 supported Ru catalyst for CO_2 methanation. After comparing with the result of CO_2 methanation over pure TiO_2 supported Ru catalyst under visible light irradiation, a possible mechanism of photo-assisted catalytic CO_2 methanation was proposed.

2. Experimental

2.1. Preparation of catalysts

The nanosized nitrogen-doped titanium dioxide ($TiO_{(2-x)}N_x$) support was made by sol-gel method. A 15 mL tetra-*n*-butyl titanate was dissolved in 50 mL absolute ethyl alcohol, and slightly yellow transparent solution A was obtained under vigorous stirring for 30 min. Solution B was gained by dissolving an amount of urea into 100 mL distilled water as well as the pH value was adjusted to 3 with 1.0 M HNO_3 solution. Then, the solution A was dropwise added into the solution B under vigorous stirring. After stirring for 3 h till the tetra-*n*-butyl titanate was hydrolyzed completely, a white emulsious solution was obtained. This hydrolysis product was dried at 80 °C and then calcined at 400 °C for 3 h, and finally a yellow $TiO_{(2-x)}N_x$ powder was obtained. Based on the amount of urea, a series of $TiO_{1.98}N_{0.02}$, $TiO_{1.91}N_{0.09}$, $TiO_{1.85}N_{0.15}$ and $TiO_{1.82}N_{0.18}$ were prepared. Here, the mass faction of nitrogen atom (x) in $TiO_{(2-x)}N_x$ was calculated by the following equation: m_{N2} (%) = 14x/(80-2x), where m_{N2} is the weight content of nitrogen element measured by Elemental Analysis.

The $TiO_{(2-x)}N_x$ supported Ru ($Ru/TiO_{(2-x)}N_x$) catalyst was prepared by impregnation-reduction method. 2.0 g $TiO_{(2-x)}N_x$ was dried in a vacuum oven at 60 °C for 2 h, and was immersed into 3.0 mL of $RuCl_3$ solution (0.1 M, 1.03 g $RuCl_3$ dissolved in 50 mL 0.1 M HCl) for 8 h at room temperature, and then was dried at 80 °C for 12 h, After Cl^- ions was removed by washing with deionized water, the obtained product was dispersed in 20 mL deionized water and reduced using a 0.1 M $NaBH_4$ solution (pH > 10 adjusted with NaOH solution) at room temperature. This was followed by

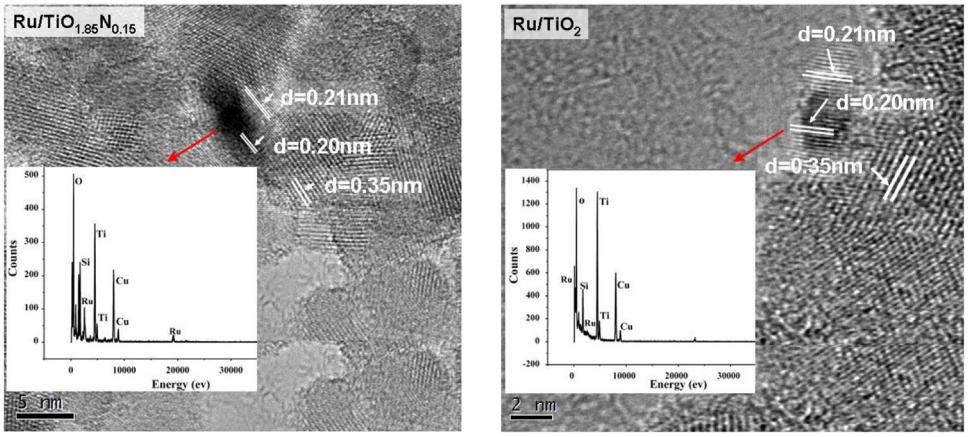

Fig. 3. TEM and EDS of $Ru/TiO_{(2-x)}N_x$ and Ru/TiO_2 samples.

washing with deionized water till the residual Na^+ and other ions below 10 ppm, and drying in a vacuum oven at 60 °C for 12 h And finally, a $Ru/TiO_{(2-x)}N_x$ sample with a theoretical Ru loading of 1.5 wt% was obtained.

Similarly, a pure TiO_2 supported Ru sample (Ru/TiO_2, TiO_2 not modified by urea) and a Al_2O_3 supported, Ru/Al_2O_3 sample were prepared according to the above impregnation-reduction method.

2.2. Catalyst characterization

Transmission electron microscopy (TEM) investigation of samples were carried out on a JEOL JEM −2010 EX with 200kv field emission gun. X-ray diffraction (XRD) of samples were recorded on Bruke D8 Advance powder X-ray diffractometer operated at 40 mA and 40 KV using Cu Ka radiation. Nitrogen isothermal stripping absorption curves of samples were measured at liquid N_2 temperature with a micromeritics ASAP 2020 BET analyzer after the sample was outgassed at vacuum and 250 °C for 4 h. Elemental Analyses (EA) of samples were tested on Vario EL cube of the Elementar Analysensysteme GmbH. UV–vis diffuse reflect spectra (UV-vis DRS) of samples were characterized on Varian Cary500 with $BaSO_4$ as internal reflectance standard. Temperature X-ray Photoelectron spectroscopy (XPS) of samples was measured on Thermo Scientific ESCALab250 spectrometer with monochromatic Al Ka as X-ray source (1486.6 eV).and with a hemispherical analyzer. The C 1s signal of 284.6 eV was used to calibrate the XPS data.

2.3. Catalytic performance

The experiment of CO_2 methanation was carried in a fixed bed flow reactor under one atmospheric pressure. And a flat-plate quartz cell (30 × 20 × 0.5 mm) as the reactor with 230 mg catalyst sample (the free space was filled with silica sand) was heated by an electric resistance board.

In the typical reaction, the catalyst sample (230 mg) with a grain size of 0.2−0.3 mm was packed in a flat-plate quartz cell (30 × 20 × 0.5 mm), and heated by an electric resistance board. The temperature of the catalyst bed was monitored by a K-type thermocouple inserted into the reactor. During the photo-thermal reaction process, visible light (435nm < λ < 465 nm, produced by a 300W Xenon lamp with a UV-reflectance filter and band-pass filter) was irradiated form the top surface of the quartz cell. For the thermal reactions (without light), the quartz cell was enclosed by Al foils to rule out light irradiations. Before reaction, the catalyst was reduced at 220 °C for 3 h in the stream of 12.0 vol% H_2-He with the flow rate of 57.0 mL min^{-1}. Then, the H_2 stream was switched to He stream, until the temperature was cooled down to room temperature. Finally, the feed stream (composed of 0.6 vol% CO_2, 2.4 vol% H_2 and the balance gas He) was fed at a total flow rate of 60.0 mL min^{-1}. The outlet stream was analyzed using an online gas chromatograph (Aglient 4890D, TDX-01) equipped with a thermal

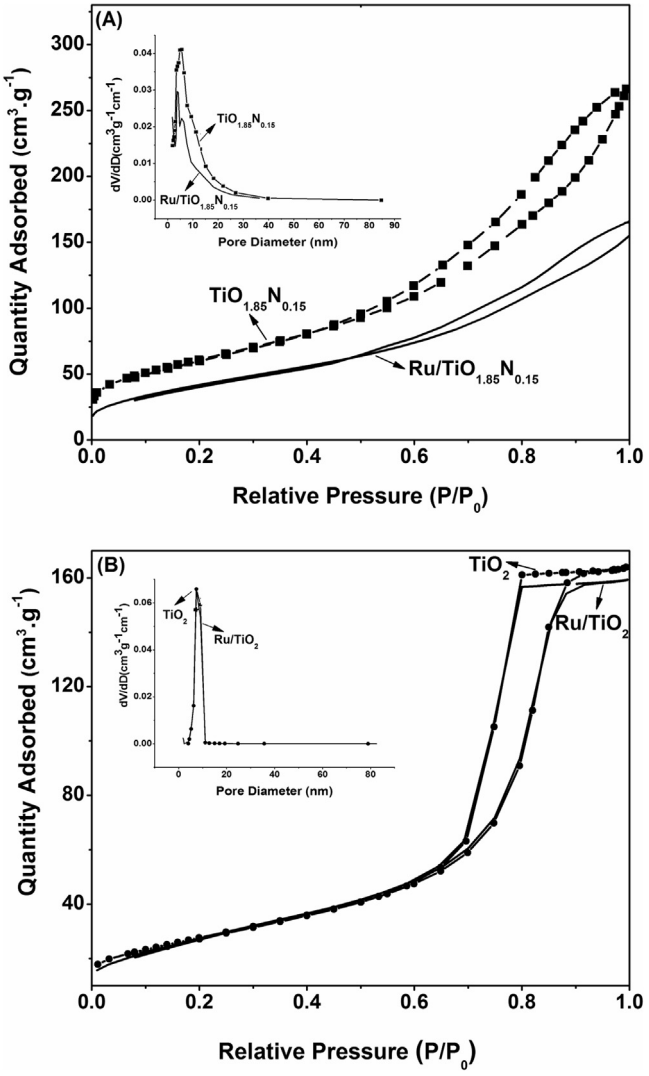

Fig. 4. N_2 adsorption–desorption isotherms and the pore size distributions (inset) plots of different samples: (A) $TiO_{1.85}N_{0.15}$ and $Ru/TiO_{1.85}N_{0.15}$; (B) TiO_2 and (d) Ru/TiO_2.

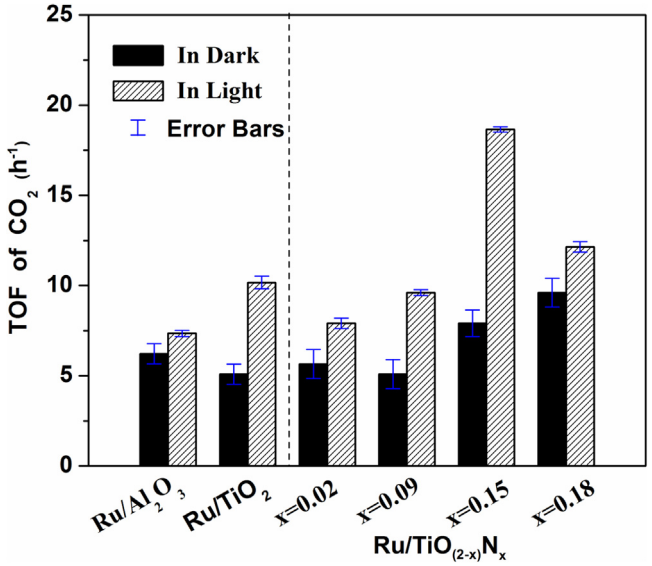

Fig. 5. The performances of CO_2 methanation over different catalyst samples at 190 °C under visible light irradiation or not.

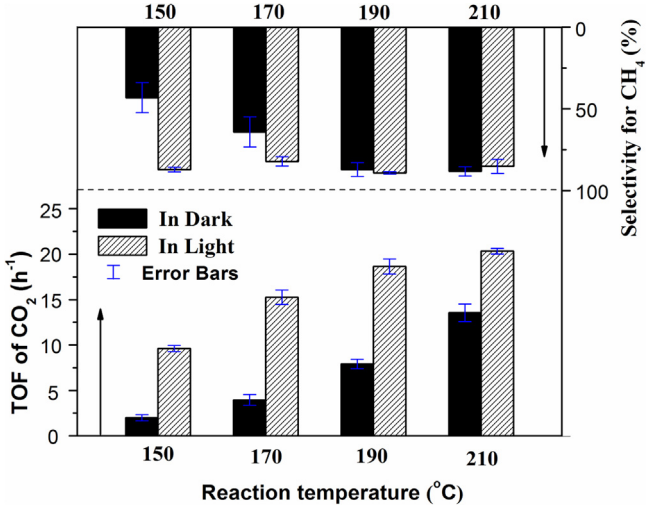

Fig. 6. The conversion of CO_2 methanation and CH_4 selectivity over $Ru/TiO_{1.85}N_{0.15}$ at different temperatures.

conductivity detector (TCD) and a flame ionization detector (FID). During the heated reaction process, enclosed with Al foils when testing the activity of the catalyst in dark, and introduced the visible light (435nm < λ < 465 nm, produced by a 300 W Xenon lamp with a UV-reflectance filter and band-pass filter) into the surface of the quartz cell when testing the activity of catalyst under visible light illumination. The change in the concentration between the inlet and outlet CO gases was used to calculate the CO conversion (X_{CO2}). For the comparison of catalytic activity, turnover frequency (TOF, the turnover number of CO to CO_2 per Ru atom per second, s^{-1}) was obtained according to the amount of Ru atoms and the space velocity. In addition, the selectivity of forming methanation (S_{CH4}) was also obtained to compare the catalytic performances of samples.

X_{CO2}, TOF and S_{CH4} were calculated using the following equations, respectively:

$$CO2(\%) = \{[CO_2]_{in}\text{-}[CO_2]_{out}\}/[CO_2]_{in}$$

$$TOF(s^{-1}) = (N_{CO} \bullet X_{CO} \bullet M_{Ru})/(Wcat \bullet W_{Ru})$$

$$S_{CH4}(\%) = [CH_4]_{out}/\{[CO_2]_{in}\text{-}[CO_2]_{out}\} = [CH_4]_{out}/\{0.60\%\text{-}[CO_2]_{out}\}$$

Where $[CO_2]_{in}$ is the inlet concentrations of CO_2 (0.6%), $[CO_2]_{out}$ is the exit concentrations of CO_2.,N_{CO2} ($mol \bullet s^{-1}$) is the molar flow of CO_2 in the feed stream, Wcat (g) is the dosage of the catalyst (0.23 g), M_{Ru} is molar mass of Ru (101.10 g mol^{-1}), W_{Ru} is the loading amount of Ru and $[CH_4]_{out}$ is the concentration of CH_4.

2.4. Chemisorptions of CO_2, CO and H_2

The chemisorption for CO_2, CO and H_2 on catalyst was respectively measured in an transform infrared spectrum (FT-IR) instrument (Nicolet Nexus, Model 670) which contains controllable environmental chamber (50 mL) with CaF_2 windows on both sides. A piece sample (20 mg) was fixed on a removable holder in the chamber. Before the test, the chamber with sample piece inside was pretreated at 200 °C in a vacuum (1.0 Pa) for 7 h. After cooling to room temperature, the absorption spectrum of sample was recorded as a reference. Then, a 5.0 mL gas (CO_2, CO or H_2) was injected into the chamber under the same controlled pressure. After 20 min, the absorption spectra of gas were collected. For testing FT-IR under visible light irradiation, a visible light (435nm < λ < 465 nm, produced by a 300 W Xenon lamp with a UV-reflectance filter and band-pass filter) was introduced onto the surface of the sample during the process of gas absorption. All spectra were recorded by a DTGS KBr detector in the transmission mode.

2.5. Temperature programed surface reaction and temperature programmed desorption

Temperature-programmed surface reaction (TPSR) measurements of samples were conducted by Micromeritics Autochem II 2910 instrument. Before tests, the powder sample (100 mg) was pretreated in purity He stream at 220 °C for 60 min and reduced in 5.0 vol%H_2-Ar stream at 220 °C for 3 h. After cooling down to room temperature in He stream (30 mL min^{-1}), the TPSR process for sample was proceeded as follows: (1) Introducing purity CO_2 (30 mL min^{-1}) into the sample for 30 min at room temperature, (2) Switching He stream till the signals of TCD and Mass signals was stable, (3) a stream of (30 mL min^{-1}) was passed through the sample with a temperature-rising rate of 5 °C min^{-1} from 25 to 350 °C. Meanwhile, the mass spectrometry (MS) analysis was performed to monitor the changes in contents of CH_4, CO_2, CO, H_2O, H_2 (*m/e* values of 16, 44, 28, 18 and 2, respectively). For testing the TPSR under visible light irraidation, the same visible light used in FT-IR testing was introduced into the sample surface during the process of adsorbing CO_2.

Temperature-programmed desorption (TPD) measurements of samples were also performed according to the processes of TPSR testing, except that a purity He stream (instead of the 5.0 vol% H_2-He stream) was passed thorough the sample during the process of heating to 350 °C.

2.6. Photoelectrochemical measurement

The electrochemical properties of the samples were performed with an electrochemical analyzer having a three-electrode configuration. A fluorine-doped tin oxide (FTO) conductive glass coated with the material film was used as a working electrode, Pt wire as a counter-electrode, and Ag/AgCl (in saturated KCl (aq)) as a reference electrode. An aqueous solution of Na_2SO_4 (0.02 M) was used as an electrolyte. The working electrodes were prepared by drop-coating, where the FTO conductive glass electrodes were first washed in an ultrasonic bath with ethanol, deionized water, and

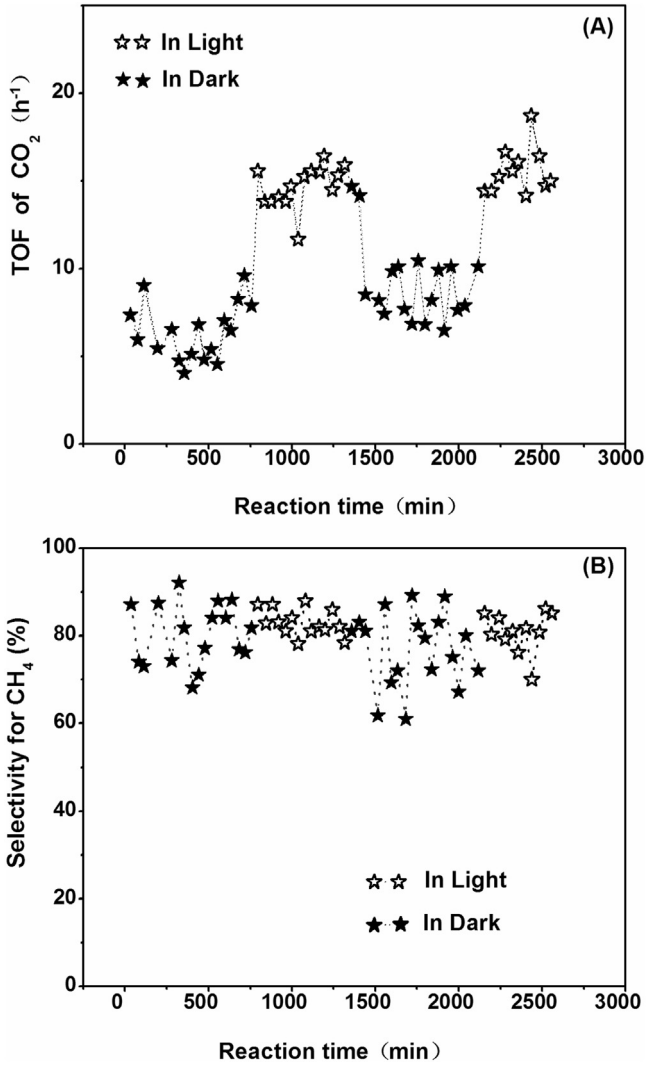

Fig. 7. CO_2 conversion (A) and CH_4 selectivity (B) as a function of reaction time over $Ru/TiO_{1.85}N_{0.15}$ at 190 °C under visible light irradiation or not.

then dried at 80 °C for 2 h. A 5 mg powder sample of TiO_2 was added to 1 mL absolute DMF to make a slurry, and the suspension was then dispersed in an ultrasonic bath for over 3 h. The resulting slurry suspension was injected uniformly onto the conductive surface of 2.5 cm × 1.0 cm FTO glass electrode with the cell size of 5 mm × 5 mm. To obtain conductive working electrodes, the non-conductive nail polish was brushed coating on the conductive surface of FTO glass. The coated FTO glass electrode was then dried at room temperature for about 12 h. The transient photocurrent response for TiO_2 stacks in the air was recorded on an electrochemical analyzer (CHI750) at the operation voltage of 0.5 V with point light as a light source. The electrochemical impedance spectroscopy (EIS) measurements were performed in a three-electrode cell and measurements recorded with CHI750.

3. Results and discussion

3.1. Catalyst characterization

Fig. 1 shows the UV–vis diffuse reflection spectroscopy (DRS) of different nitrogen content $TiO_{(2-x)}N_x$ samples. The pure TiO_2 sample only exhibited at the absorption at UV region (λ < 400 nm), while the $TiO_{(2-x)}N_x$ samples exhibited the absorption at visible light region (i.e., a red shift of optical absorption band edge). Moreover, the red-shift extent of $TiO_{(2-x)}N_x$ sample was enlarged with the increasing nitrogen content (the optical absorption band edge expanded from near 430 nm to 600 nm with the nitrogen atom fraction from 0.02 to 0.18), which consistent with the results of reported literature about nitrogen doping titanium dioxide [39,40]. Meanwhile, $TiO_{(2-x)}N_x$ samples still exhibited the TiO_2 intrinsic characteristic for absorbing UV light (λ < 400 nm) [33].

Table 1
The textural data of $TiO_{1.85}N_{0.15}$, $Ru/TiO_{1.85}N_{0.15}$, TiO_2 and Ru/TiO_2 samples.

Sample	BET surface area (m^2g^{-1})	Pore diameter (nm)	Pore volume ($cm^3\ g^{-1}$)
$TiO_{1.85}N_{0.15}$	220.82	7.46	0.41
$Ru/TiO_{1.85}N_{0.15}$	156.57	6.86	0.27
TiO_2	99.44	10.20	0.25
Ru/TiO_2	102.30	9.64	0.25

Fig. 2 shows the XRD patterns ofTiO_2, $TiO_{1.85}N_{0.15}$, Ru/TiO_2 and Ru/TiO $TiO_{1.85}N_{0.15}$ samples. All samples presented the main crystal structure of TiO_2 anatase (including the crystal planes of (101), (004), (200), (105), (211), (118), (116), (220) and (215)) as well as a little crystal structure of TiO_2 brookite (the crystal planes of (121)). However, no characteristic diffraction peaks of Ru species were observed over Ru/TiO_2 and $Ru/TiO_{1.85}N_{0.15}$ samples, indicating that the low loading amount of Ru species are highly dispersed on the surface of TiO_2 or $TiO_{1.85}N_{0.15}$ [33].

The result of TEM and EDS (Fig. 3) shows that single Ru (111) particles (d = 0.20 nm) [33] were deposited on the bi-crystalline planes (d = 0.21 nm or 0.19 nm) of brookite TiO_2 to form a matching interface over both TiO_2 and $TiO_{1.85}N_{0.15}$ samples. .Yang et al. [41] have proposed that the matching interface structure between TiO_2 and Pt nanoparticles could promote the interface electron transference when Pt(111) supported on brookite TiO_2 surfaces directly. Based on this viewpoint, the matching interface structure between Ru and brookite TiO_2 maybe also promote the electron transfer between Ru and the support. In addition, two samples both presented a typical (101) plane face of anatase TiO_2 (d = 0.35 nm) [33].

Fig. 4 shows that loading Ru on $TiO_{1.85}N_{0.15}$ or TiO_2 still remained the ink bottle mesoporous structure of $TiO_{1.85}N_{0.15}$ or TiO_2 support, which can be attributed to the IV type of nitrogen isothermal stripping absorption curves. However, the structure of TiO_2 was somewhat different from that of $TiO_{1.85}N_{0.15}$. As compared to TiO_2, $TiO_{1.85}N_{0.15}$ owned a more uniform pore size, a smaller aperture and a larger specific surface area (see Table 1). Moreover, loading Ru on $TiO_{1.85}N_{0.15}$ could decrease the BET specific surface area and aperture of $Ru/TiO_{1.85}N_{0.15}$ support, but loading Ru on TiO_2 did not decrease those of Ru/TiO_2 (see Table 1).

3.2. Catalytic performances

Fig. 5 shows the performances of CO_2 methanation at 190 °C over Ru catalysts supported on different supports under visible light irradiation or not. To indentify the differences of catalysts with varies nitrogen contents, the Ru loading amounts were kept at 1.5 wt% according to our previous work about the CO methanation over Ru/TiO_2 [33]. In addition, the wavelength of visible light was selected at 435–465 nm according to the absorption band edge of samples in Fig. 1. In fact, the comparative results of catalyst samples with different loading contents of Ru also show that the $Ru/TiO_{1.85}N_{0.15}$ owned a better catalytic performance (see Fig.s1 in Supplementary information (SI)). Moreover, the comparative results at different reaction temperatures also indicate that the $Ru/TiO_{1.85}N_{0.15}$ catalysts exhibited a better catalytic performance at 190 °C (see Fig. s2 and Fig. s3 in SI)

As compared to the Ru/Al_2O_3 and Ru/TiO_2 samples, the $Ru/TiO_{(2-x)}N_x$ samples with a low content of nitrogen

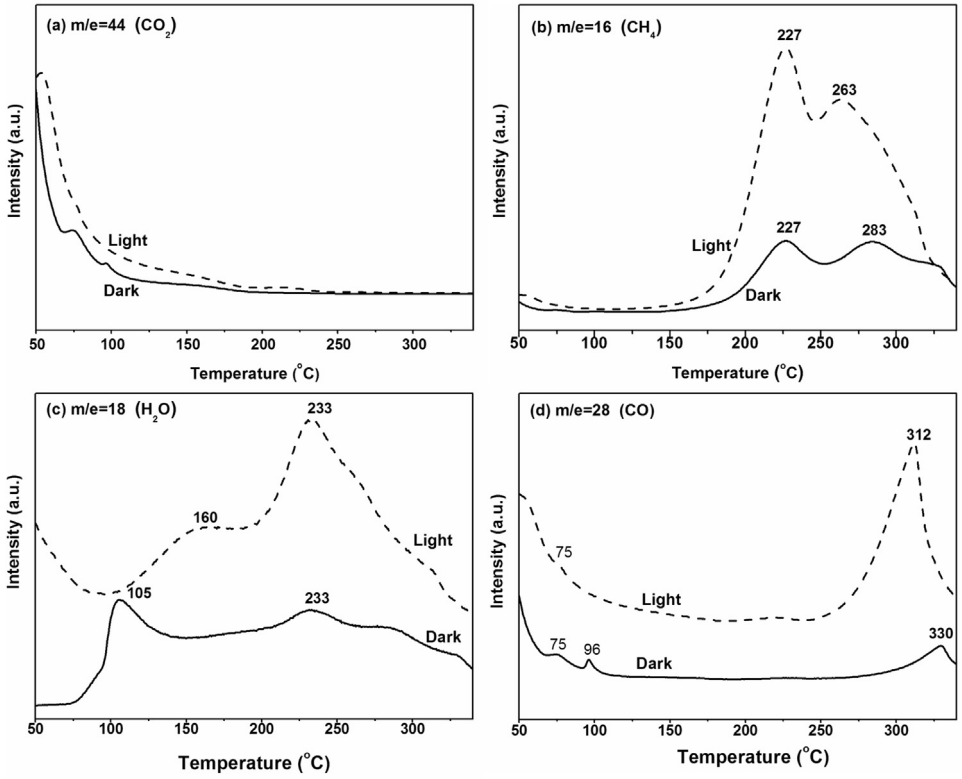

Fig. 8. TCD and Mass signals of (a) CO_2 (m/e = 44), (b) CH_4 (m/e = 16), (c) H_2O (m/e = 18), and (d) CO (m/e = 28) during the H_2-TPSR process over $Ru/TiO_{1.85}N_{0.15}$ after pre-adsorbing CO_2 for 30 min under visible light irradiation (Light) or in dark (Dark).

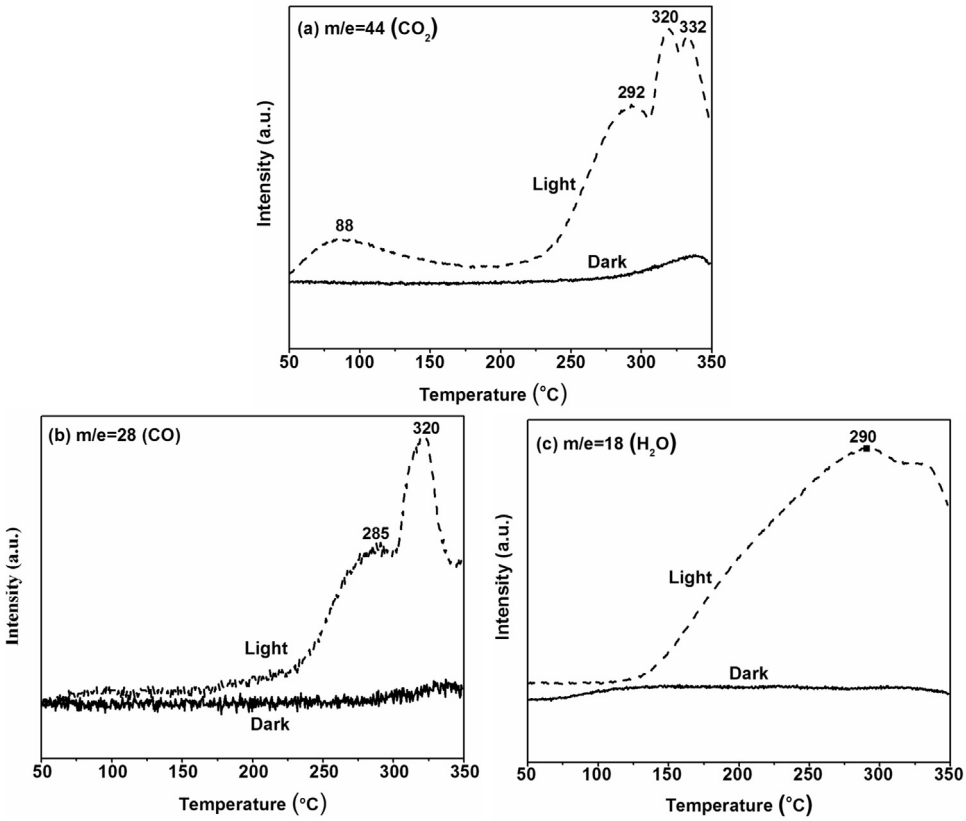

Fig. 9. Mass signals of (a) CO_2 (m/e = 44), (b) CO (m/e = 28) and (c) H_2O (m/e = 18) during the TPD process over $Ru/TiO_{1.85}N_{0.15}$ after adsorbing CO_2 for 30 min under visible light irradiation (Light) or in dark (Dark).

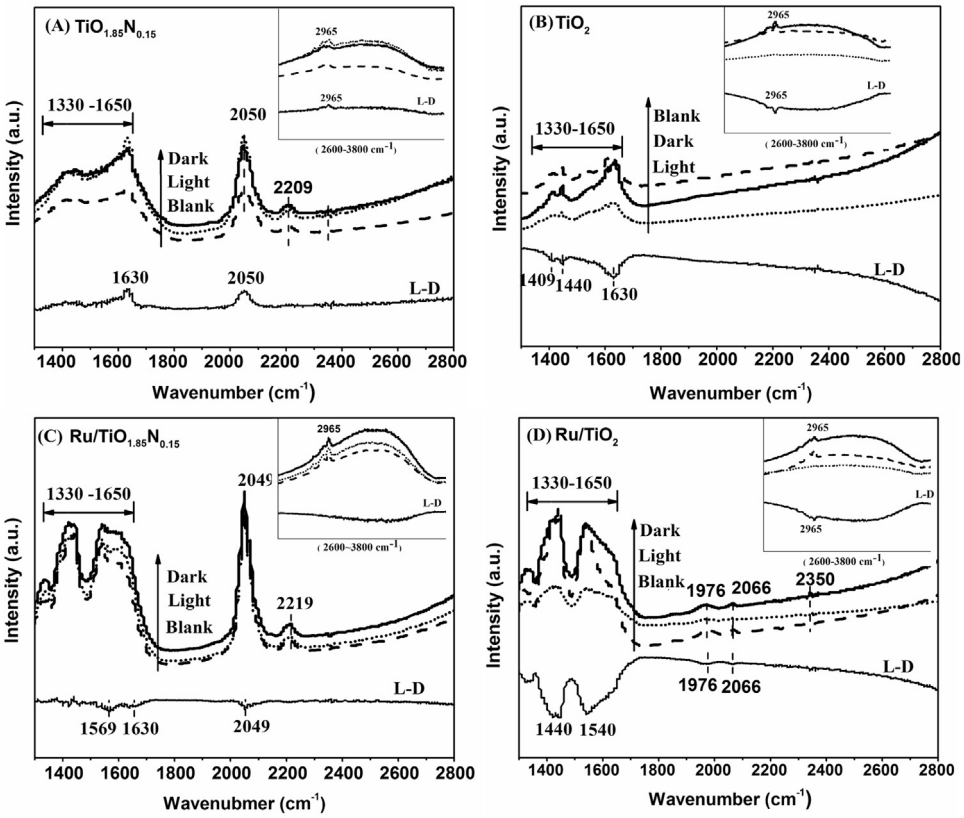

Fig. 10. FT-IR spectra of adsorbing CO_2 over (A) $Ru/TiO_{1.85}N_{0.15}$, (B) $TiO_{1.85}N_{0.15}$, (C) Ru/TiO_2 and (D) TiO_2 samples under different conditions: (Blank) before adsorbing CO_2, (Dark) after adsorbing CO_2 in dark and (Light) after adsorbing CO_2 under visible light irradiation. The curve L-D is curve Dark subtracted from curve Light, denoting the difference of each sample adsorbing CO_2 with visible light and that in dark. Here, the adsorption peak at 2965 cm^{-1} over each sample could be attributed to the high vacuum grease species used for sealing the reacting tube in the experiment.

($Ru/TiO_{1.98}N_{0.02}$ and $Ru/TiO_{1.91}N_{0.09}$) did not exhibit a better catalytic activities for CO_2 methanation in dark, but the $Ru/TiO_{(2-x)}N_x$ samples with a high content of nitrogen ($Ru/TiO_{1.85}N_{0.15}$ and $Ru/TiO_{1.82}N_{0.18}$) presented a higher catalytic activity in dark. With the introduction of the visible light, the conversions of CO_2 increased over all samples, even if over Ru/Al_2O_3. Moreover, $Ru/TiO_{1.85}N_{0.15}$ showed the best catalytic activity under visible light irradiation. The results indicate that the nitrogen-doped TiO_2 support can promote the thermo-catalytic activity of Ru nanoparticles for CO_2 methanation, and introducing visible light can further promote its catalytic activity. However, the promoted effect of visible light on CO_2 methanation apparently decreases over the excessive nitrogen-doped sample ($Ru/TiO_{1.82}N_{0.18}$).

This promoted effect of nitrogen doping into TiO_2 on CO_2 methanation may be associated with the formation of oxygen vacancy in $TiO_{(2-x)}N_x$. Zhang et al. [42] have suggested that the removal of oxygen atoms is easier than nitrogen atoms, and the required energy of removing oxygen atom to form vacancy in N-doped TiO_2 can reduce from 4.3 to 0.6 eV by DFT calculation in the report of Valentin et al. [43]. These existed oxygen vacancies can capture the photo-generated electrons, which affect the migration of charge carriers [44,45] and then the catalytic activity, especially under visible light irradiation. However, Upham et al. [46] have reported that the excessive amounts of oxygen vacancy on the surface of $Ru_{0.05}Ce_{0.95}O_x$ may reduce the catalytic activity for CO_2 methanation. This may be one reason for $Ru/TiO_{1.82}N_{0.18}$ exhibiting a lower catalytic activity than $Ru/TiO_{1.85}N_{0.15}$ under visible light irradiation (see Fig. 5).

In addition, the Ru/TiO_2 catalyst also showed an obviously photo-enhanced performance for CO_2 methanation under visible light irradiation (TOF value of CO_2 increasing from 5.0 h^{-1} in dark to 10.0 h^{-1} under visible light irradiation), which may be attributed to the existence of oxygen vacancies [42] and Ti^{3+} species [47] formed during the preparing process, such as vacuum heat treatment in reducing atmosphere. These oxygen vacancies and Ti^{3+} species can form a localized state (a shallow energy level) in the bottom of TiO_2 conduction band, resulting in the absorption of visible light [48]. Moreover, the oxygen vacancies on the surface can capture electrons to form excitons due to the nanosize effect of TiO_2 nanoparticles, which can be also excited by a longer wavelength light than that of the intrinsic absorption band [49]. Note that this photo-assisted effect over Ru/TiO_2 seemed to be stronger than that over $Ru/TiO_{1.98}N_{0.02}$, $Ru/TiO_{1.91}N_{0.06}$ or $Ru/TiO_{1.82}N_{0.18}$ sample (but weaker than that over $Ru/TiO_{1.85}N_{0.15}$). That is to say, the TiO_2 doped with too little or too much nitrogen could not benefit to exert the photo-assisted effect on CO_2 methanation over Ru catalyst as compared to the pure TiO_2 support. This phenomenon may be ascribed to the change in the amount of oxygen vacancies existed at different $Ru/TiO_{(2-x)}N_x$ samples. A detailed explanation would be described in Section 3.6 of the proposed reaction process.

However, introducing visible light seemed not to promote the CO_2 conversion over Ru/Al_2O_3 which cannot be excited by visible light. As can be seen, the photo-enhanced performances of the catalysts mainly originate from the light-excitation of TiO_2 and $TiO_{(2-x)}N_x$ supports.

Furthermore, comparing the catalytic activities of $Ru/TiO_{1.85}N_{0.15}$ sample for CO_2 methanation at different temperatures (see Fig. 6), it can be seen that $Ru/TiO_{1.85}N_{0.15}$ exhibited the better CO_2 conversion and CH_4 selectivity at 190 °C under visible light irradiation. Moreover, introducing visible light

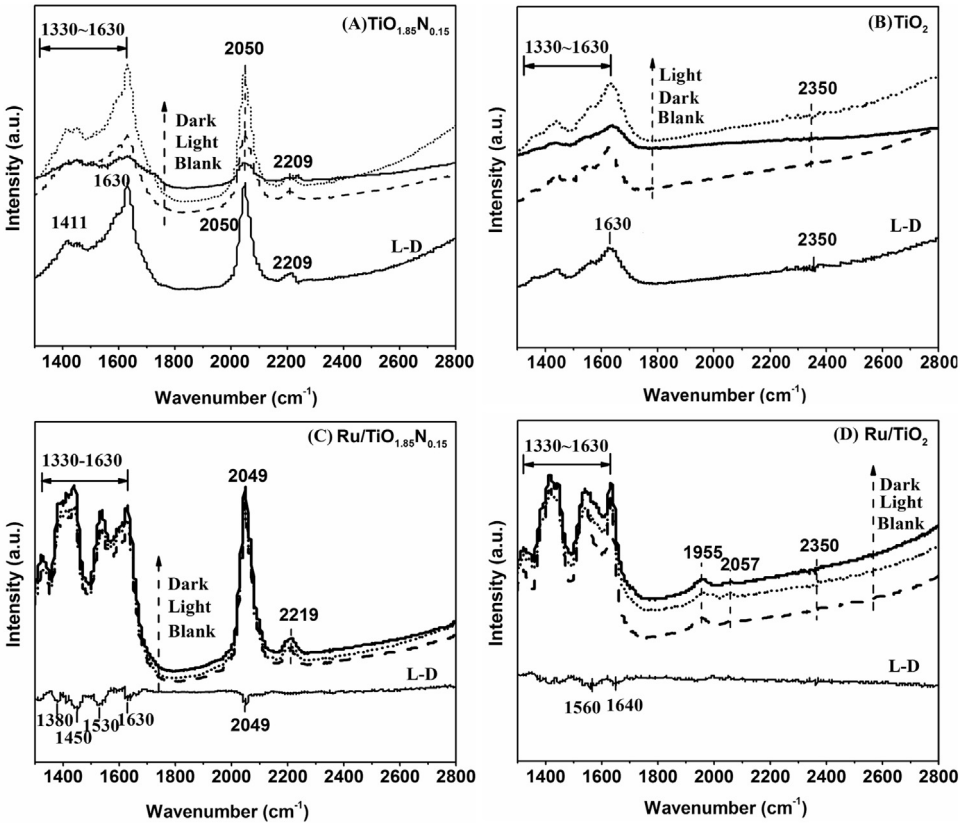

Fig. 11. FT-IR spectra of adsorbing CO over (A) $Ru/TiO_{1.85}N_{0.15}$, (B) $TiO_{1.85}N_{0.15}$, (C) Ru/TiO_2 and (D) TiO_2 samples under different conditions: (Blank) before adsorbing CO, (Dark) after adsorbing CO in dark and (Light) after adsorbing CO under visible light irradiation. The curve L-D is curve Dark subtracted from curve Light, denoting the difference of each sample adsorbing CO with visible light and that in dark.

could enhance the duration and stability of catalytic activity of $Ru/TiO_{1.85}N_{0.15}$. As seen in Fig. 7, the TOF values of CO_2 were maintained at about 7.0 h^{-1} but the CH_4 selectivity were fluctuated between 70.0%∼90.0% in dark. With the introduction of visible light, the TOF values of CO_2 increased up to 15.0 h^{-1} and the CH_4 selectivity were also stably kept at about 80% during the reaction process. Although the removal of visible light led to the decrease of CO_2 conversion and the fluctuation of CH_4 selectivity, the reintroduction of visible light could increase the TOF value of CO_2 and keep the stability of CH_4 selectivity again. This indicates that visible light can steadily promote the CO_2 conversion into CH_4. According to the thermo-catalytic reaction process of CO_2 mehtanation over Ru catalyst [24], this photo-assisted effect may be somewhat related with the formation of intermediate active species. The detailed studies were presented step by step in the following sections.

3.3. Chemisorption behaviors of CO_2 and H_2

Considering that CO_2 methanation process will be somewhat dependent on the adsorption and activation of reactants, the chemisorption behaviors of CO_2 and H_2 over $Ru/TiO_{1.85}N_{0.15}$ were investigated by TPSR, TPD and FT-IR measurements, respectively.

3.3.1. TPSR-Mass testing

Fig. 8 shows the TPSR results of $Ru/TiO_{1.85}N_{0.15}$ for adsorbing CO_2 and H_2 in order under visible light irradiation or not. It can be seen that CO_2 signals decreased but the signals of CH_4 and H_2O increased with the increase of temperatures in the two cases of adsorbing CO_2 both in dark and under visible light irradiation, indicating that CO_2 can be transformed into CH_4 above a temperature. As compared to that of sample pre-adsorbing CO_2 in dark, the desorption peak of CH_4 (mass signal) made a slight shift to a lower temperature concomitant with an obviously increased peak area in the case of pre-adsorbing CO_2 under visible light irradiation. This indicates that the introducing visible light during the process of adsorbing CO_2 can significantly promote the CO_2 methanation over $Ru/TiO_{1.85}N_{0.15}$. Moreover, the mass signals of CO were also observed during the two TPSR processes, but the desorption temperature of CO was higher than that of CH_4, respectively. This shows CO can be formed during the process of CO_2 to CH_4 (i.e., CO may be the reaction intermediate of CO_2 methanation), and the CH_4 selectivity would decline with the increase of reaction temperature. Similarly, the CO signal under visible light irradiation was larger than that in dark, indicating that visible light can promote the formation of CO. However, it cannot be identified whether the formed CO intermediates were originated from the desorbed product of CO_2 or the reduced product of CO_2 by H_2, due to the presence of H_2 during the TPSR process. Therefore, the TPD tests of $Ru/TiO_{1.85}N_{0.15}$ adsorbing CO_2 under visible light irradiation or not were also conducted.

3.3.2. TPD-Mass testing

As seen from the TPD results of $Ru/TiO_{(2-x)}N_x$ adsorbing CO_2 in Fig. 9, a small peak of CO_2 desorption was also observed at a high temperature (above 300 °C) for the case of adsorbing CO_2 in dark, but two larger peaks of CO_2 desorption could be observed at a low temperature range (near 80 °C) and a high temperature range (above 280 °C), respectively, indicating that visible light can promote the adsorption of CO_2 at $Ru/TiO_{1.85}N_{0.15}$. Moreover, a stronger intensity of CO and H_2O signal could be observed accompanied by CO_2 desorption at the high temperature in the case

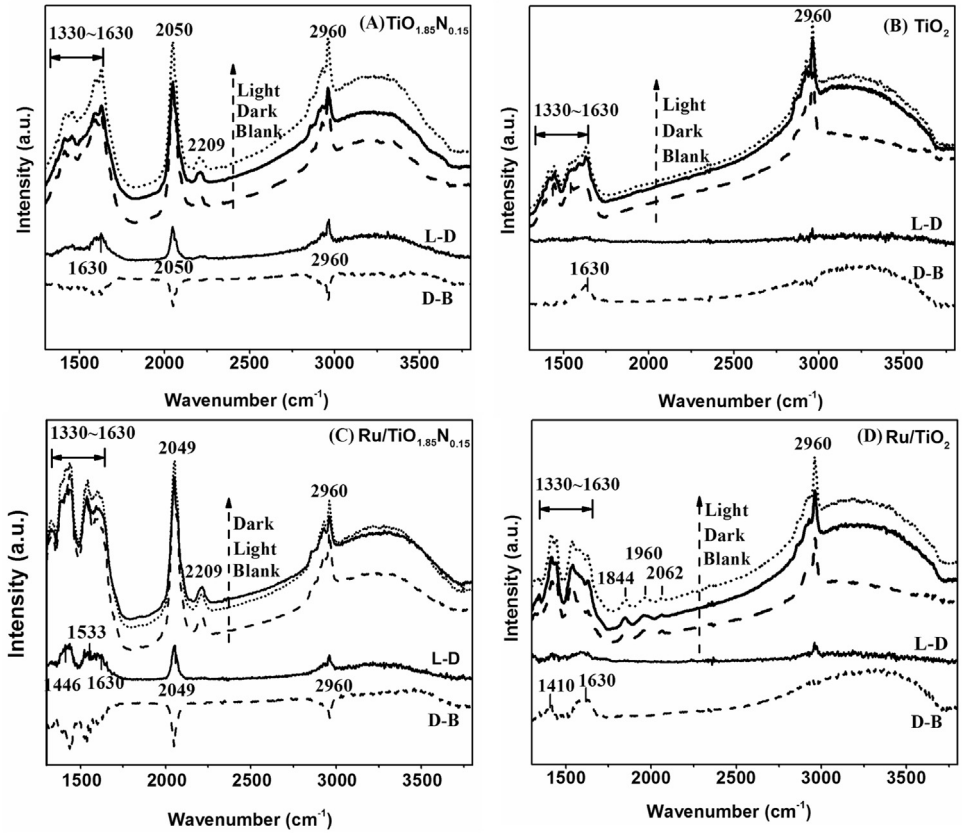

Fig. 12. FT-IR spectra of adsorbing H_2 over (A) $Ru/TiO_{1.85}N_{0.15}$, (B) $TiO_{1.85}N_{0.15}$, (C) Ru/TiO_2 and (D) TiO_2 samples under different conditions: (Blank) before adsorbing H_2, (Dark) after adsorbing H_2 in dark and (Light) after adsorbing H_2 under visible light irradiation, respectively. The curve L-D is curve Dark subtracted from curve Light, the curve D-B is curve Blank subtracted from curve Dark. Here, the adsorption peak at 2960 cm^{-1} over each sample could be attributed to the high vacuum grease species used for sealing the reacting tube in the experiment.

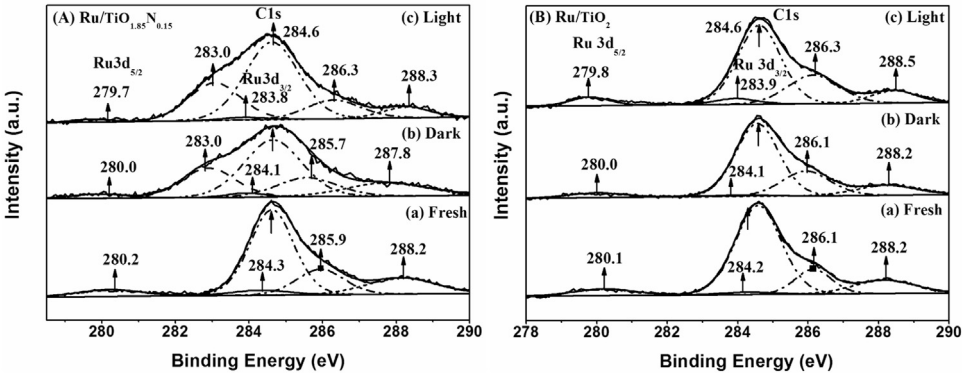

Fig. 13. High-resolution XPS spectra of C1 s and Ru3d of (A) $Ru/TiO_{1.85}N_{0.15}$ and (B) Ru/TiO_2 samples under different treatments: (Fresh) after H_2 pre-treatment at 220 °C; (Dark) after reacted at 190 °C for 8 h in dark; (Light) after reacted at 190 °C for 8 h under visible light irradiation.

of visible light irradiation, indicating that the adsorbed CO at $Ru/TiO_{1.85}N_{0.15}$ can be directly transformed into the CO species. In fact, Karelovic et al. [50] have reported that the adsorbed $Rh_2(CO)_3$ species could be observed when CO_2 was adsorbed at $Rh/\gamma\text{-}Al_2O_3$, and the adsorbed $Ru^{x+}(CO)_x$ species also appeared after CO_2 was adsorbed at Ru/Zeolite or Ru/Al_2O_3.

However, the CO mass signals seemed not to be changed during the TPSR and TPD testing process for Ru/TiO_2 under visible light irradiation or not (see Fig. s3 and Fig. s4 in SI), indicating that no stable CO intermediates can be formed by the CO_2 adsorption at Ru/TiO_2. Although the introduction of visible light also could promote the adsorption of CO_2 at Ru/TiO_2, this promoted effect is much less than that of $Ru/TiO_{1.85}N_{0.15}$.

In order to further demonstrate the above results, a FT-IR test for CO_2 adsorption was performed over $Ru/TiO_{1.85}N_{0.15}$, which was compared with that over Ru/TiO_2, $TiO_{1.85}N_{0.15}$ and TiO_2 samples, respectively.

3.3.3. FT-IR test for CO_2 adsorption

Fig. 10 shows the FT-IR results of CO_2 adsorption over $TiO_{1.85}N_{0.15}$, TiO_2, $Ru/TiO_{(2-x)}N_x$ and Ru/TiO_2,samples under visible light irradiation or dark. All samples appeared the following peaks after adsorbing CO_2: The symmetric OCO stretching (ν_s(OCO)) peak of bidentate formate species at 1330 cm^{-1}, the asymmetric OCO stretching (ν_a(OCO)) peak of bridging bidentate formate species at 1585 cm^{-1} [51], the peak of the adsorbed carbonate species

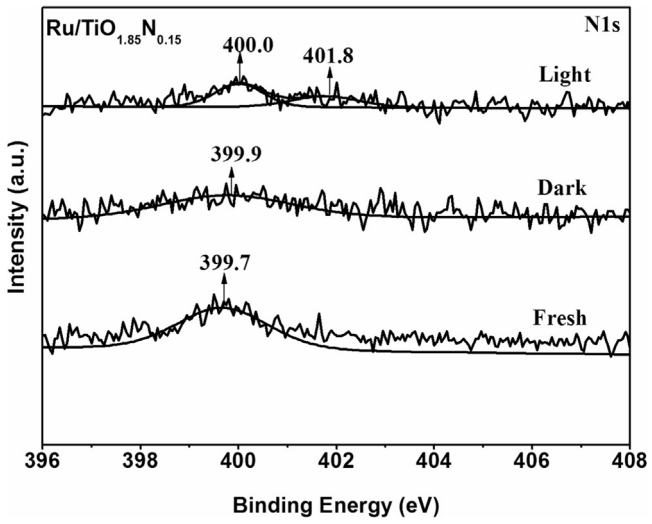

Fig. 14. High-resolution XPS spectra N1 s of $Ru/TiO_{1.85}N_{0.15}$ sample under different treatments: (Fresh) after H_2 pre-treatment at 220 °C; (Dark) after reacted at 190 °C for 8 h in dark; (Light) after reacted at 190 °C for 8 h under visible light irradiation.

(CO_3^{2-}) at 1440 cm^{-1}, the peak of the asymmetric bicarbonate species (HCO_3^-) in 1540–1630 cm^{-1} [52–55], and the peak of the broad peak of adsorbed water in 3000–4000 cm^{-1} [56]. However, the presence of visible light could cause the different changes in these peaks over different samples (see the L-D curves in each samples).

For $TiO_{1.85}N_{0.15}$ sample, the introduction of visible light obviously promoted the increase of the adsorption peaks at 1440 cm^{-1}, 1540 cm^{-1}–1630 cm^{-1}, assigned to the carbonate and bicarbonate species [52–55] (see the L-D curve in Fig. 10A). But for TiO_2 sample, the adsorption peaks of carbonate and bicarbonate species at 1440 cm^{-1} and 1630 cm^{-1}, decreased apparently with the introduction of visible light (see the L-D curve in Fig. 10B). Moreover, $TiO_{(2-x)}N_x$ exhibited a more adsorbed water in 3000–4000 cm^{-1} than TiO_2 (see the top right image in two samples in Fig. 10). According to the report of Marmood et al. [57], the CO_2 methanation reaction over Ru/TiO_2 would mainly proceed as the following steps: The adsorbed CO_2 molecules first react with the adsorbed H_2O molecules to form the carbonate and bicarbonate species, then convert to adsorbed CO species and finally hydrogenate to produce CH_4, Therefore, a more formation of carbonate and bicarbonate species over $TiO_{1.85}N_{0.15}$ than TiO_2 means that $TiO_{1.85}N_{0.15}$ support is favorable for adsorbing CO_2 and H_2O and then the formation of the intermediates compared with TiO_2 support, especially under visible light irradiation. However, for the $Ru/TiO_{1.85}N_{0.15}$ and Ru/TiO_2 samples, the introduction of visible light weakened the adsorption band of carbonate and bicarbonate species at 1330–1650 cm^{-1} (see curves L-D in Fig. 10C and D), indicating that the presence of Ru may be favorable for the further transformation of intermediates into other species (e.g., CO).

In addition, two adsorption peaks at 1976 and 2066 cm^{-1}, assigned to the adsorbed CO species [58–60], could be observed over Ru/TiO_2 sample (Fig. 10D). Similarly, two observed adsorption peaks at 2049 and 2219 cm^{-1} over $Ru/TiO_{1.85}N_{0.15}$ sample (Fig. 10C) may be also assigned to the adsorbed CO species at Ru sites (the shifts of two peaks can be attributed to the two different supports). However, the two samples themselves appeared the CO species before adsorbing CO_2 (see curve in Fig. 10B and D), and the CO_2 adsorption in dark did not cause an obvious increase of the adsorbed CO species. Maybe this is because some CO_2 in air are adsorbed at the surface of the two samples during the preparation process. Although the samples were treated in vacuum at 200 °C, the CO species formed by the adsorbed CO_2 in air is too stable to remove, which also suppresses the formation of new CO species induced by adsorbing CO_2 in dark. This may be one reason that the CO_2 adsorption peaks at 2350 cm^{-1} over all samples were very weaker (transforming into CO and other species). Note that the $TiO_{1.85}N_{0.15}$ sample itself also appeared the peaks at 2049 cm^{-1} and 2209 cm^{-1} before adsorbing CO_2, indicating that the $TiO_{1.85}N_{0.15}$ support without loading Ru can also adsorb CO_2 in air and then translate it into the CO species. Note that these CO species may be also introduced by the formation of the coordination bond carbonyls (C=O → M) induced by urea reacting with Ti^{4+} ions during the hydrolysis process of tetrabutyl titanate [61]. However, no CO species could be observed over TiO_2 sample (see Fig. 10D), indicating that TiO_2 support itself cannot transform the adsorbed CO_2 into CO species.

With the introduction of visible light, the above peaks of CO species were weakened over $Ru/TiO_{1.85}N_{0.15}$ and Ru/TiO_2 (see curve (L-D) in Fig. 10C and D), indicating that the formed CO species can be further transformed into other species under visible light irradiation. However, the peaks of CO species over $TiO_{1.85}N_{0.15}$ were enhanced with the introduction of visible light ((see curve (L-D) in Fig. 10A), indicating that the visible light can promote the formation of CO species but not to promote its further transforming into other species over $TiO_{1.85}N_{0.15}$. This also indicates that Ru nanoparticles are mainly responsible for CO_2 methanation.

The above results shows that the $TiO_{(2-x)}N_x$ support itself can transform the adsorbed CO_2 into the CO species (as the intermediates of CO_2 methanation), which can be further promoted by the visible light. However, the CO_2 adsorbed at TiO_2 support cannot be transformed into CO species over TiO_2, even if under visible light irradiation. Maybe that is why $Ru/TiO_{(2-x)}N_x$ exhibits a higher catalytic activity for CO_2 methanation than Ru/TiO_2 both in dark and under visible light irradiation.

3.3.4. *Fourier transform infrared spectroscopy (FT-IR) of CO*

In order to confirm that the observed peaks at 2209 and 2047 cm^{-1} in Fig. 10 can be assigned to the CO species adsorbed on the samples' surface, the FT-IR results of adsorbing CO (instead of CO_2) were also tested over the above four samples under visible light irradiation or not.

As shown in Fig. 11, the respective FT-IR spectrum of adsorbing CO were very similar to that of adsorbing CO_2 in Fig. 10 over each sample, indicating that the formed species (including the CO species) by adsorbing CO may be the same as those by adsorbing CO_2. Especially for $TiO_{1.85)}N_{x0.15}$ sample, the change of two peaks at 2050 $cm^{-1}$and 2209 cm^{-1} induced by visible light was larger than that of adsorbing CO_2 (see the L-D curve in Figs. 10A and 11A), further indicating that these two peaks in both Figs. 10 and 11 can be assigned to the adsorbed CO species. This also means that visible light can promote the adsorption of CO at $TiO_{1.85}N_{0.15}$ surface. However, the absorption peaks of CO were not observed over TiO_2 sample after adsorbing CO (see Fig. 11D), but the peaks at 1411 cm^{-1} and 1630 cm^{-1} assigned to the carbonate and bicarbonate species [52–55] were obviously enhanced, indicating that the adsorbed CO at TiO_2 maybe converts into other species. For $Ru/TiO_{1.85}N_{0.15}$ sample, introducing visible light seemed not to promote the adsorption of CO (see curve L-D in Fig. 11C), which may be attributed to the further transformation of CO into other intermediates at Ru sites. Also, this phenomenon occurred on the Ru/TiO_2 sample (see curve L-D in Fig. 11D).

The above FT-IR results of adsorbing CO further confirm that the peaks at 2050 cm^{-1} and 2219 cm^{-1} over $Ru/TiO_{1.85}N_{x0.15}$, Ru/TiO_2 and $TiO_{1.85}N_{x0.15}$ samples in Fig. 10A–C can be actually assigned to the CO species formed by the adsorbed CO_2 at Ru or $TiO_{1.85}N_{x0.15}$ sites. In fact, Tóth et al. [62] have also reported that a CO species adsorbed at Rh sites can be observed during the process of CO_2

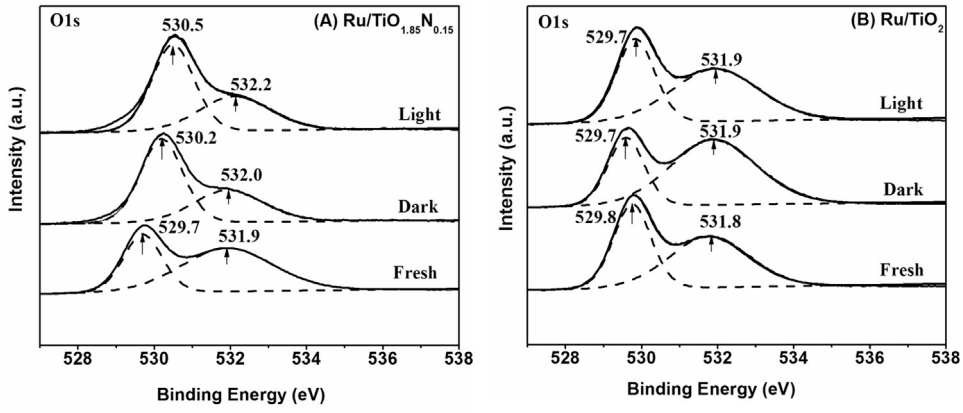

Fig. 15. High-resolution XPS spectra of O1 s of (A) $Ru/TiO_{1.85}N_{0.15}$ and (B) Ru/TiO_2 samples under different treatments: (Fresh) after H_2 pre-treatment at 220 °C; (Dark) after reacted at 190 °C for 8 h in dark; (Light) after reacted at 190 °C for 8 h under visible light irradiation.

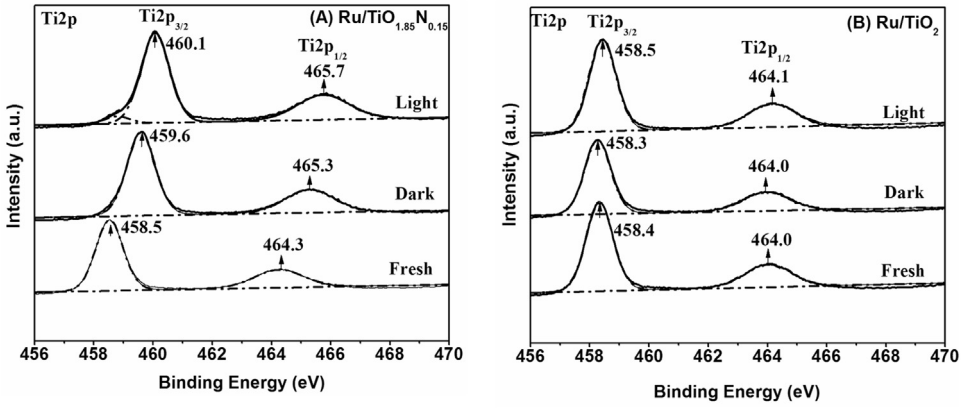

Fig. 16. High-resolution XPS spectra of Ti2p of (A) $Ru/TiO_{1.85}N_{0.15}$ and (B) Ru/TiO_2 samples under different treatments: (Fresh) after H_2 pre-treatment at 220 °C; (Dark) after reacted at 190 °C for 8 h in dark; (Light) after reacted at 190 °C for 8 h under visible light irradiation.

methanation over Rh/TiO_2 catalysts. Meanwhile, this adsorbed CO species also make an interaction with the oxygen vacancy of TiO_2 adjacent to Ru sites. Stefan et al. [63] have also proposed that the CO species adsorbed at Cu sites would participate the CO_2 methanation over $Au\text{-}Cu/TiO_2$ catalyst as the intermediate. As can be seen, the CO_2 may be involved into the process of its methanation over $Ru/TiO_{(2-x)}N_x$ by forming CO species at the surface oxygen vacancies of $TiO_{(2-x)}N_x$ support.

3.3.5. *Fourier transform infrared spectroscopy of H_2 (FT-IR)*

Considering that H_2 as a reactant will also take part in the process of CO_2 methanation, the FT-IR tests of H_2 adsorption over $Ru/TiO_{1.85}N_{0.15}$, Ru/TiO_2, $TiO_{1.85}N_{0.15}$ and TiO_2 were also performed respectively.

As shown in Fig. 12, although the IR vibrating peak of H_2 could not be detected due to the symmetry structure of H_2 molecules, the H_2 adsorption could cause the change of FT-IR spectra over each sample. For $TiO_{1.85}N_{x0.15}$ and $Ru/TiO_{1.85}N_{x0.15}$ samples, the H_2 adsorption in dark could lead to the intensity decrease of the peaks at 1330–1630 cm^{-1}, 2049 cm^{-1} (see curve D-B in Fig. 12A and B), assigned to the carbonate (or bicarbonate) species and CO species, respectively, but seemed not to cause the obvious changes of the adsorbed water (see the broad area in 3000–4000 cm^{-1} in curve D-B). With the introduction of visible light during the process of adsorbing H_2, the absorption peaks of carbonate or bicarbonate species, the adsorbed CO species and the adsorbed water species were obviously enhanced (see curve L-D in Fig. 12A and B). This indicates that the adsorbed hydrogen species over $Ru/TiO_{1.85}N_{x0.15}$ and $TiO_{1.85}N_{x0.15}$ samples in dark maybe directly react with the carbonate, bicarbonate and CO species, resulting in the decrease of these intermediates, while adding visible light could promote the reformation of these species, also including H_2O species. For Ru/TiO_2 and TiO_2 sample, the adsorption peaks of carbonate and bicarbonate species at 1330–1630 cm^{-1} and the adsorbed water species at 3000–4000 cm^{-1} were obviously enhanced after adsorbing H_2 in dark (see curve D-B in Fig. 12C and D), but almost were invariable with the introduction of visible light (see curve in Fig. 12C and D). This indicates that the adsorbed hydrogen species over Ru/TiO_2 and TiO_2 samples in dark maybe could promote the formation of H_2O, carbonate, bicarbonate and CO species, but adding visible light could not further promote the formation of these species, especially over TiO_2 sample. In addition, the peaks at 1844, 1960 and 2060 cm^{-1} may be attributed to the M-CO species formed during the process of loading Ru nanoparticles.

Apparently, these different behaviors of adsorbing H_2 over two group samples could be attributed to the different structure of $TiO_{1.85}N_{0.15}$ and TiO_2 support. For $TiO_{1.85}N_{0.15}$ support, due to the existence of CO species at $TiO_{1.85}N_{0.15}$ sites, the adsorbed hydrogen species maybe directly react with CO species and other intermediates, resulting in the decrease of these intermediates. For TiO_2 support, due to no CO species formed at TiO_2 sites, the adsorbed hydrogen species maybe directly with the surface hydroxyl species and lattice oxygen of TiO_2 to form the adsorbed H_2O molecules as described in our previous study [64]. In fact, it was also reported that the adsorbed H_2 at TiO_2 surface will form H_2O or the chemical bonds with the oxygen species [65–67]. This formed H_2O will

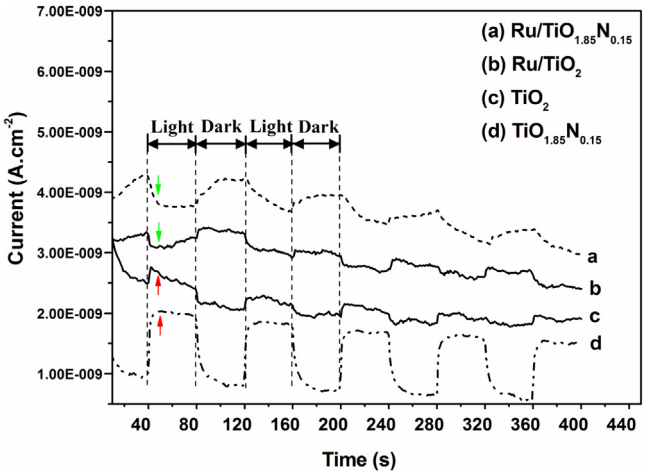

Fig. 17. Transient photocurrent responses of (a) $Ru/TiO_{1.85}N_{0.15}$, (b) Ru/TiO_2, (c) TiO_2 and (d) $TiO_{1.85}N_{0.15}$ samples in 0.1 M Na_2SO_4 aqueous solution under visible light irradiation (Light) or in dark (Dark).

further promote the transformation of the adsorbed CO_2 into the carbonate or bicarbonate species at TiO_2 surface (TPD result in Fig. 9 also shows that the adsorbed CO_2 or its intermediates was too strong to be completely desorbed at the pretreatment temperature of 200 °C).

Under the visible light irradiation, since the surface oxygen atom in $TiO_{(2-x)}N_x$ is more easily removed than that in TiO_2 due to the weaker Ti-O bond in the former [42,43], the adsorbed H_2 maybe react with the lattice oxygen of $TiO_{(2-x)}N_x$ to generate the oxygen vacancies with concomitant formation of surface H_2O species. The formed oxygen vacancies maybe further promote the adsorbed CO_2 to transform into CO species and other intermediates. In fact, Aziz et al. [68] have ever proposed that the oxygen vacancies of support can promote the adsorption of CO_2 and then form CO during the process of CO_2 methanation over the Ni catalyst supported on mesoporous silica nanoparticles (MSN). However, visible light could not promote the formation of oxygen vacancies in the presence of H_2 due to the stable Ti-O bond (of course the adsorbed H_2 should promote the formation of oxygen vacancies under ultra-violet light irradiation [69]). Therefore, no obvious changes of surface H_2O and carbonate or bicarbonate species could be observed over TiO_2 sample under visible light irradiation.

Noted that the change in the absorption bands of 1330–1450 cm^{-1} (i.e. the carbonate or bicarbonate species) over $Ru/TiO_{1.85}N_{0.15}$ was larger than that over $TiO_{1.85}N_{0.15}$ (comparing two curves D-B in Fig. 12A and B), which may be attributed to the hydrogen spillover behavior from Ru to $TiO_{1.85}N_{0.15}$. For the process of CO_2 methanation over the TiO_2 supported group VIII metal catalysts, Raupp et al. [70] have ever proposed that the dissociative adsorbed H at metal nanoparticles can spillover onto the support, and then directly reacting with the active carbon or carbonaceous intermediates adsorbed at the TiO_2-metal interface.

Considering that the intermediates of CO_2 existed on the surface of all blank samples before adsorbing H_2, the FT-IR results in Fig. 12 could be regarded as the reaction process of CO_2 or its intermediates with H_2 at room temperature under visible light irradiation or not. According to the above FT-IR results of adsorbing H_2, the CO_2 methanation process over $Ru/TiO_{1.85}N_{0.15}$ may be different from that over Ru/TiO_2. For the CO_2 methanation process over Ru/TiO_2, the adsorbed H_2 maybe first react with the surface oxygen of TiO_2 to form H_2O species, which then react with the adsorbed CO_2 to form the carbonate, bicarbonate species and CO species. For the CO_2 methanation process over $Ru/TiO_{1.85}N_{0.15}$, the adsorbed H_2 maybe directly react with CO or other active carbon species (induced by the oxygen vacancies of $TiO_{1.85}N_{0.15}$) at $TiO_{1.85}N_{0.15}$ instead of forming H_2O. Under visible light irradiation, the $TiO_{1.85}N_{0.15}$ support can be photo-excited and then generate more surface oxygen vacancies, resulting in the more formation of CO species and then the promoted CO_2 methanation. On the contrary, TiO_2 cannot be produced the new oxygen vacancies under visible light irradiation, resulting in no new surface H_2O species being formed in the presence of H_2. Thus, visible light cannot obviously promote CO_2 methanation over Ru/TiO_2.

Table 2
Relative contents of two oxygen species over $Ru/TiO_{1.85}N_{0.15}$ and Ru/TiO_2 samples under the different reaction conditions.

Samples		Relative contents of two oxygen species	
		Lattice Oxygen	Hydroxyl groups or Hydroxides
$Ru/TiO_{1.85}N_{0.15}$	Fresh	0.36	0.64
	In Dark	0.61	0.39
	In Light	0.59	0.41
Ru/TiO_2	Fresh	0.44	0.56
	In Dark	0.31	0.69
	In Light	0.42	0.58

As can be seen, the better catalytic activity of $Ru/TiO_{(2-x)}N_x$ may be attributed to $TiO_{(2-x)}N_x$ owning the more surface oxygen vacancies and the subsequent promoted formation of CO species. Moreover, the visible light could further promote the above behaviors. To confirm this deduction and also investigate the intermediates from CO_2, the XPS tests for $Ru/TiO_{1.85}N_{0.15}$ and Ru/TiO_2 samples under different reaction conditions were compared.

3.4. X-ray photoelectron spectroscopy (XPS)

Fig. 13 shows the High-resolution XPS spectra of C1 s and Ru3d of $Ru/TiO_{1.85}N_{0.15}$ and Ru/TiO_2 samples. The C1 s feature of the two fresh $Ru/TiO_{1.85}N_{0.15}$ and Ru/TiO_2 samples could be deconvolved into three peaks at 284.6 eV, 285.3 eV and 288.3 eV, assigned to the standard carbon species (graphite), hydrocarbons and carbonates (two latter were presumably picked up during exposed to the air or produced during the low-temperature drying process) [33]. As compared to the fresh sample, the reacted $Ru/TiO_{1.85}N_{0.15}$ samples both in dark and in light exhibited a new C1 s peak at 283.0 eV, which can be assigned to the carbon species bound to Ru atoms (C-Ru) [71]. Moreover, the new C1 s peak over the reacted sample in light seemed to be higher than that over the reacted sample in dark. The increase in the electron density of carbon species means that more stable carbon active intermediates originated from CO_2 can be formed at the sample surface, which can be further promoted under visible light irradiation. On the other hand, the carbon species adsorbed at the fresh sample maybe also accepts electrons during the reaction process. However, the changes of carbon species seemed not to appear over the reacted Ru/TiO_2 sample in dark or under visible light irradiation. This indicates that the $TiO_{1.85}N_{0.15}$ support can benefit to translate the adsorbed CO_2 into the activity carbon species as compared to TiO_2 support, and adding visible light can further promote this process. In fact, Aziz et al. [68] has found that the high catalytic activity of Ni/MSN in CO_2 methanation comes from the positive function of support that plays on the formation of surface carbon species, and the surface carbon species can interact with atomic hydrogen to form methane. This result further shows that the formed active carbon species at $TiO_{1.85}N_{0.15}$ support may be mainly responsible for the better activity of $Ru/TiO_{1.85}N_{0.15}$ for CO_2 methanation. In fact, as can be seen from Fig. 6, the introduction of visible light could lead to the increase in the selectivity of CO_2 into CH_4 over $Ru/TiO_{1.85}N_{0.15}$ catalyst, which was coincident with the increase in the amount of active carbon species (the peak

at 283.0 eV in Fig. 13A) over the reacted $Ru/TiO_{1.85}N_{0.15}$ sample in the light condition.

In addition, the Ru3d signals could be also observed over the two fresh $Ru/TiO_{1.85}N_{0.15}$ and Ru/TiO_2 samples [59] (the respective BE of $Ru3d_{5/2}$ at 280.1 and 280.3 eV, but the two corresponding $Ru3d_{3/2}$ peaks overlapped by C1 s peaks). Both the reacted samples in dark exhibited a lower BE value than the respective fresh sample (from 280.3 to 280.0 eV for $Ru/TiO_{1.85}N_{0.15}$ and from 280.1 to 279.9 eV for Ru/TiO_2, respectively), which may be attributed to the further reducing of Ru species by H_2 during the reaction process. Moreover, both the two reacted samples under visible light irradiation exhibited a lower BE value of Ru3d5/2 than the corresponding sample reacted in dark, respectively. This may be because the photo-generated electrons can transfer from $TiO_{1.85}N_{0.15}$ or TiO_2 to Ru due to the former owning a higher Fermi energy than the latter [72].

Note that the $Ru3d_{5/2}$ intensities of the two reacted $Ru/TiO_{1.85}N_{0.15}$ samples seemed to be weaker than that of the fresh sample. Maybe this is because the Ru nanoparticles were somewhat covered by the formed carbon species during the reaction process. However, the intensity of Ru $3d/_{5/2}$ of the three Ru/TiO_2 samples were almost stable due to no the formation of carbon active species over TiO_2 support.

Fig. 14 shows the XPS result of N1 s of $Ru/TiO_{1.85}N_{0.15}$ samples under the different treatment conditions. Only one N1 s peak centered at 399.7 eV could be observed on the fresh $Ru/TiO_{1.85}N_{0.15}$ sample, which can be attributed to the nitrogen doped into TiO_2 [73]. After reacted in dark, the BE value of N1 s of the $Ru/TiO_{1.85}N_{0.15}$ sample made a high shift from 399.7 to 399.9 eV, indicating the decrease in the surface electron density of N atom during the reaction process. With the introduction of visible light during the reaction process, the BE value of N1 s of the reacted sample further become larger, and even was splitted into two values at 400.0 eV and 401.8 eV, respectively. This means that two kinds of doped N species maybe existed at the sample surface [73]. According to the report of Wang et al. [74], the peak at 402.0 eV can be assigned to the N species in the N-Ti-O structure. Since the oxygen atom can be easily removed than nitrogen atom (i.e., forming oxygen vacancies) under visible light irradiation in the N-Ti-O structure [42,73], the nitrogen atom needs to offer more electrons to compensate for the electrons provided by oxygen atom, resulting in the higher BE of N1s. In addition, the decrease in surface electron density of N species may be also attributed to the electron transfer from $TiO_{1.85}N_{0.15}$ to Ru nanoparticles.

Fig. 15 shows the High-resolution XPS spectra of O1s of $Ru/TiO_{1.85}N_{0.15}$ and Ru/TiO_2samples. Each sample exhibited two apparent peaks of O1s, which the peak at 529.7-530.5 eV was assigned to the lattice oxygen [75], and the other at 531.8-532.2 eV was assigned to the surface hydroxyl groups or hydroxides [76]. For $Ru/TiO_{(2-x)}N_x$ sample, the BE value of O1s attributed to the lattice oxygen make a high shift from 529.7 to 530.2 eV after reacted in dark, and further to 530.5 eV after reacted under visible light irradiation, indicating the decrease in the surface electron density of the lattice oxygen over the reacted $Ru/TiO_{1.85}N_{0.15}$ sample as compared to the fresh sample. Göpel et al. [77] have reported that the formation of oxygen vacancy of TiO_2 can cause the increase in the BE of O1s located in lattice oxygen. This means that some oxygen vacancies will be formed at the surface of $TiO_{(2-x)}N_x$ during the reaction of CO_2 methanation over $Ru/TiO_{(2-x)}N_x$, especially under visible light irradiation. However, the unchanged BE value of O1s attributed to the lattice oxygen in the three Ru/TiO_2 samples means that the lattice oxygen of TiO_2 might be somewhat stable during the reaction process under visible irradiation or not.

In addition, the BE value of O1s attributed to the surface hydroxyls or hydroxides also make a high shift from 531.9 eV up to 530.0 eV after reacted in dark, and further up to 532.2 eV after reacted under visible light irradiation, indicating the decrease in surface electron density of O atom attributed to the hydroxyls over the reacted $Ru/TiO_{1.85}N_{0.15}$ sample as compared to the fresh sample. This behavior of surface hydroxyls may also be attributed to the formation of surface oxygen vacancies similar to that of the lattice oxygen. Moreover, the formation of carbonate or bicarbonate species, induced by the surface hydroxyl interacting with CO_2, maybe also causes the decrease in surface electron density of hydroxyls during the process of CO_2 methanation. Since visible light can promote the formation of surface oxygen vacancies, so the electron density of the oxygen atoms in surface hydroxyls further decreases over the reacted $Ru/TiO_{1.85}N_{0.15}$ sample in light. However, the BE value of O1s in the surface hydroxyls for the three Ru/TiO_2 samples almost be unchanged.

Note that the ratio of O1s peak area of hydroxyl species to that of lattice oxygen over the $Ru/TiO_{1.85}N_{0.15}$ sample decreased during the reaction process in dark (Table 2), indicating that some hydroxyl species can be consumed by CO_2 to form other active intermediates (finally into the carbon species in the presence of H_2). While the increase of this ratio in visible light means that H_2 can react with the lattice oxygen in $TiO_{1.85}N_{0.15}$ to form more surface hydroxyl species due to the photo-excitation of $TiO_{1.85}N_{0.15}$. On the contrary, the ratio of the hydroxyl species to the lattice oxygen in Ru/TiO_2 would increase after reacting in dark, showing that more hydroxyl species would be formed during the reaction process but not to be consumed by CO_2 to form other active intermediates. Furthermore, adding visible light into the reaction system could lead to the decrease of hydroxyl species at Ru/TiO_2 surface, indicating that visible light maybe promotes the transformation of hydroxyl species into other active intermediates, but did not promote the formation of surface hydroxyl species induced by H_2 reacting with lattice oxygen over Ru/TiO_2. These results are consistent with the FT-IR result of adsorbing H_2 in Fig. 12.

This above explanation can be further confirmed by the XPS results of Ti2p in $Ru/TiO_{1.85}N_{0.15}$ samples treated by different conditions. As shown in Fig. 16A, the BE value of $Ti2p_{3/2}$ make a high shift from 458.5 up to 459.6 eV after reacted in dark, and further up to 460.1 eV after reacted under visible light irradiation. Chandra et al. [78] have ever reported that the Ti^{4+} species in TiO_2-SiO_2 with different coordination structures would present the different BE value of Ti2p. The BE of $Ti2p_{3/2}$ at 458.5 eV for the fresh sample can be assigned to the Ti^{4+} species with an octahedral coordination structure (one Ti atom coordinated with the adjacent six atoms), and that at 459.6 or 460.1 eV for the reacted sample to the Ti^{4+} species with a tetrahedral coordination structure (atom coordinated with the adjacent four atoms). This result indicates that the Ti^{4+} species with the octahedral structure in the fresh $Ru/TiO_{1.85}N_{0.15}$ sample, could be transformed into the tetrahedral structure due to the removal of the coordinated oxygen during the reaction process under visible light irradiation or not. Note that the electron transfer from $TiO_{1.85}N_{0.15}$ to Ru could also cause the increase in BE values of both Ti2p and O1s during the reaction process. Since the increased BE of O1s (from 531.9 to 532.0 eV of O1s in Fig. 15A) was much less than that of Ti2p (from 458.8 to 459.6 eV for Ti2p3/2 in Fig. 16A), we think that the increased BE of Ti2p may be mainly attributed to the change of coordination structure. However, no obvious change of the BE value of Ti2p could not be observed for the three Ru/TiO_2 samples (see Fig. 16B), indicating that the coordinated structure keeps stable during the reaction process. This result further demonstrated that the oxygen vacancies could be easily formed at the $TiO_{(2-x)}N_x$ surface during the reaction process of CO_2 methanation, especially under visible light irradiation.

All of the above XPS explanations can be concluded as follows: (I) During the reaction process (especially under visible light irradiation), the lattice oxygen in $TiO_{1.85}N_{0.15}$ can be easily removed to

form the surface oxygen vacancies and then the surface hydroxyl species, resulting in change of surface electron density of O, Ti and N atoms. (II) CO_2 adsorbed at the surface oxygen vacancies in $TiO_{1.85}N_{0.15}$ could react with the surface OH^- to form the carbon active intermediates and then the CO species, which further react with the dissociative H to form the active carbon species (C1s at 283.0 eV over $Ru/TiO_{1.85}N_{0.15}$; (III) Under visible light irradiation, the photo-generated electrons form $TiO_{1.85}N_{0.15}$ or TiO_2 will transfer to Ru nanoparticles, resulting the increase of Ru surface electron density and the decrease of $TiO_{1.85}N_{0.15}$ surface electron density (including Ti, O, N). This electron transfer behavior can also be regarded as the strong metal-support interaction (SMSI) effect between Ru and $TiO_{1.85}N_{0.15}$ or TiO_2. However, the electron transfer behavior from TiO_2 to Ru induced by visible light cannot be apparently observed by the decrease in electron density of Ti and O atoms (i.e., the increase in BE value of Ti2p and O1s). To further confirm the electron transfer between Ru and $TiO_{1.85}N_{0.15}$ or TiO_2 support, a photocurrent test for $Ru/TiO_{1.85}N_{0.15}$, Ru/TiO_2, $TiO_{1.85}N_{0.15}$, TiO_2 were conducted, respectively.

3.5. Photocurrent test

As shown in Fig. 17, both $TiO_{1.85}N_{0.15}$ and TiO_2 samples produced an obvious positive photocurrent ($I_{photo} > 0$, $I_{photo} = I_{Light} - I_{Dark}$) under visible light irradiation (see curves d and c), and the photocurrent of the former was much stronger than that of the latter. Moreover, the $Ru/TiO_{1.85}N_{0.15}$ and Ru/TiO_2 samples exhibited a larger current in dark than the $TiO_{1.85}N_{0.15}$ and TiO_2 support sample, respectively, but exhibited a negative photocurrent (the decreased current, $I_{photo} < 0$) with the introduction of visible light (see curves a and b), and also the absolute value of photocurrent change of $Ru/TiO_{1.85}N_{0.15}$ was larger than that of Ru/TiO_2. This indicates that loading Ru into $TiO_{1.85}N_{0.15}$ or TiO_2 could promote the electron transfer within the film inner or at the interface of film and the conducting FTO substrate. However, the photo-generated electrons from $TiO_{1.85}N_{0.15}$ or TiO_2 induced by visible light maybe transfer onto the Ru surface opposite to the direction of electron transfer in the testing system (i.e., the direction of electron transfer between film and FTO substrate), resulting in the decrease of current under visible light irradiation.

For the extrinsic excitation behavior of TiO_2 induced by visible light, it is reported that its photo-generated electrons could be captured by the surface oxygen vacancies [49,79], resulting in the decrease in Fermi level of TiO_2. However, this drooped energy level could be higher than the Fermi level of FTO substrate, thus some photo-generated electrons of TiO_2 could still transfer into the FTO substrate (consistent with the direction of electron transfer forming current), and the increased current was observed over TiO_2 sample under visible light irradiation. When Ru was supported on TiO_2 surface, both the surface oxygen vacancies and Ru nanoparticles would accept the photo-generated electrons, resulting in the further decrease in the Fermi level of TiO_2 (even lower than that of FTO substrates). Here, some electrons maybe transfer from FTO to TiO_2, which opposites to the direction of electron transfer forming current. Therefore, a decrease in current was observed on the Ru/TiO_2 with the introduction of visible light. For $Ru/TiO_{1.85}N_{0.15}$ sample, the photo-generated electrons of $TiO_{1.85}N_{0.15}$ induced by visible light could also be captured by the surface oxygen vacancies and Ru nanoparticles, a similar behavior into that of Ru/TiO_2 maybe also occurred during the photocurrent testing process. This result shows that Ru could actually accept the photo-generated electrons from $TiO_{(2-x)}N_x$ or TiO_2 induced by visible light.

Note that adding UV light could cause the positive change of photocurrent for both $Ru/TiO_{1.85}N_{0.15}$ and Ru/TiO_2, consistent with the results of $TiO_{1.85}N_{0.15}$ and TiO_2 samples (see Fig. s6 in SI). This indicates that the presence of Ru nanoparticles did not change the transfer direction of photo-generated electrons induced by the intrinsic excitation of TiO_2 (TiO_2 structure also existed in $TiO_{(2-x)}N_x$). Moreover, the extrinsic excitation behavior of $TiO_{(2-x)}N_x$ or TiO_2 induced by visible light may be different from the intrinsic excitation behavior of TiO_2 induced by UV light. A detailed explanation needs to be further studied.

3.6. Proposed reaction process

According to the above results and analyses, the CO_2 methanation process over $Ru/TiO_{(2-x)}N_x$ may be different from that over Ru/TiO_2. For the CO_2 methanation over $Ru/TiO_{(2-x)}N_x$, the surface oxygen vacancies existed on $TiO_{(2-x)}N_x$ surface can benefit to the interaction between surface hydroxyls and CO_2, resulting in the formation of carbonate or bicarbonate species and finally the CO species [80]. Subsequently, the formed CO species maybe react with the dissociative H adsorbed at Ru sites (or the H spillovered onto $TiO_{(2-x)}N_x$) to form CH_4. Here, the dissociative H maybe first react with the active CO species to form other carbon active species ($2TiO_{(2-x)}N_x\text{-}H + TiO_{(2-x)}N_x - CO \rightarrow TiO_{(2-x)}N_x\text{-}C + TiO_{(2-x)}N_x + H_2O$), and then form into the methane ($TiO_{(2-x)}N_x\text{-}C + 4Ru\text{-}H \rightarrow TiO_{(2-x)}N_x + Ru + CH_4$). Under visible light irradiation, the $TiO_{(2-x)}N_x$ support can be excited to generate more surface oxygen vacancies (especially in the presence of H_2), resulting in the more formation of CO species and then the promoted CO_2 methanation. In addition, the photo-generated electrons induced by $TiO_{(2-x)}N_x$ maybe also transfer onto the Ru nanoparticles, resulting in the increase in surface electron density of Ru nanoparticles. The rich electrons at Ru surface could transfer to the adsorbed CO_2, resulting in the polarization of CO_2 and the bending of O-C-O bond (i.e., promotes the activation of CO_2) [81]. This above proposed processes of CO_2 methanation over $Ru/TiO_{(2-x)}N_x$ can be also described as Fig. 18A.

For the CO_2 methanation over Ru/TiO_2, the adsorbed H_2 maybe first react with the lattice oxygen of TiO_2 to form H_2O species, which then react with the adsorbed CO_2 to form the carbonate, bicarbonate species and CO species. Under visible light irradiation, no new oxygen vacancies and surface H_2O species can be formed in the presence of H_2 due to TiO_2 not being intrinsic-excited. Here, only the photo-generated electrons induced by extrinsic excitation of TiO_2 can transfer onto Ru naoparticles, and the formed Ru sites with rich electrons can facilitates the polarization and activation of CO_2 adsorbed at its surface. This proposed process of CO_2 methanation over Ru/TiO_2 may be described as Fig. 18B.

The two above proposed mechanisms could also explain the following phenomenon in Fig. 5. The TiO_2 doped with too little or too much nitrogen could not benefit to exert the photo-assisted effect on CO_2 methanation over Ru catalyst as compared to the pure TiO_2 support. According to the reaction process described in Fig. 18, besides the enhanced visible light absorption, the oxygen vacancies maybe also play two other opposite roles on CO_2 methanation: On one hand, the oxygen vacancies would be prone to adsorb CO_2 and its activation into CO and the subsequent active carbon species. On the other hand, the oxygen vacancies maybe also accept the photo-generated electrons, resulting in a less electron transfer to Ru nanoparticles and then a lower activity. For the Ru catalyst supported on $TiO_{(2-x)}N_x$ doped with a less nitrogen ($Ru/TiO_{1.98}N_{0.02}$ or $Ru/TiO_{1.91}N_{0.09}$), a less amount of oxygen vacancies would be formed under visible light irradiation, resulting in the former positive role being too low. For the Ru catalyst supported on $TiO_{(2-x)}N_x$ doped with a more nitrogen ($Ru/TiO_{1.82}N_{0.18}$), a more amount of oxygen vacancies would be formed under visible light irradiation, resulting in the latter negative role being too stronger. Therefore, only the Ru catalyst supported on $TiO_{(2-x)}N_x$ doped with a suitable nitrogen ($Ru/TiO_{1.85}N_{0.15}$) could balance the two opposite roles, which resulted in the stronger photo-assisted effect on CO_2 metha-

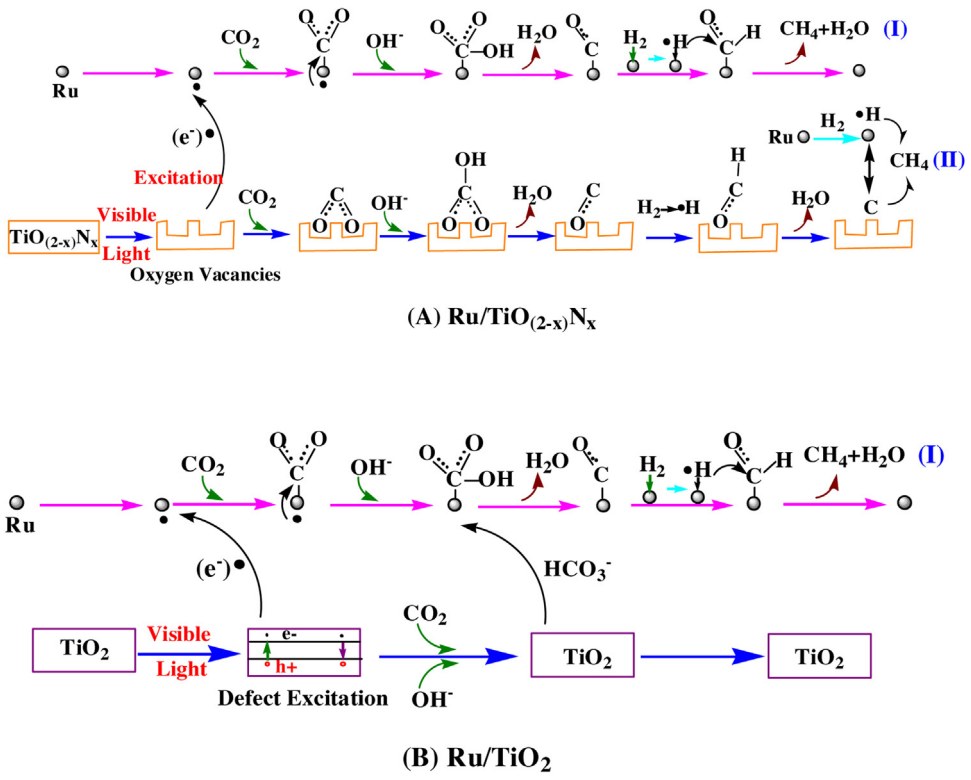

Fig. 18. The proposed process of CO_2 methanation over (A) $Ru/TiO_{(2-x)}N_x$ and (B) Ru/TiO_2 under visible light irradiation.

nation than that of Ru/TiO_2 (no new oxygen vacancies formed at TiO_2 surface under visible light irradiation).

4. Conclusions

From the present investigation the following conclusions can be drawn:

- $Ru/TiO_{(2-x)}N_x$ exhibits a better catalytic activity for CO_2 methanation than Ru/TiO_2 under visible light irradiation or not, and the promoted effect of visible light on the former is much more significant than that on the latter.
- For the CO_2 metanation over $Ru/TiO_{(2-x)}N_x$ catalyst, the photo-assisted effect of visible light mainly come from two cases: On the one hand, the $TiO_{(2-x)}N_x$ itself can be favorable for the adsorption of CO_2 and its activation into the CO species (as the intermediates of CO_2 methanation reaction), and the visible light can further promote this behavior by forming the oxygen vacancies over $TiO_{(2-x)}N_x$. On the other hand, the photo-generated electrons of $TiO_{(2-x)}N_x$ induced by visible light can transfer to the Ru nanoparticles, resulting in the increase in the surface electron density of Ru and then the promoted adsorption and activation of CO_2.
- For the CO_2 methanation over Ru/TiO_2 catalyst, TiO_2 itself cannot transform the adsorbed CO_2 into the CO intermediates, which resulted in a lower thermo-catalytic activity for CO_2 methanation. Under visible light irradiation, the extrinsic excitation of TiO_2 cannot promote the formation of new surface oxygen vacancies at TiO_2 surface, but still can excite TiO_2 to produce the electrons. These photo-generated electrons can transfer from TiO_2 to Ru surface to increase the surface electron density of Ru sites, resulting in a promoted adsorption and activation of CO_2 at Ru sites and then the promoted CO_2 methanation.
- This study shows that improving the light absorbing property of a supported metal catalyst by modifying support maybe improve its photo-assisted effect for a thermo-catalytic reaction. This promoted effect can be mainly dependent on the electron transfer behavior between metal and support (i.e., the SIMI effect). Therefore, how to activate support may be one possible approach to improve the catalytic performance of the supported metal catalysts.

Acknowledgment

This work was financially supported by the National Natural Science Foundation of China (no. 21273037), the National Basic Research Program of China (973 Program, no. 2014CB239303) and Science & Technology Plan Project of Fujian Province (no. 2014Y2003).

Appendix A. Supplementary data

Supplementary data associated with this article can be found, in the online version, at http://dx.doi.org/10.1016/j.apcatb.2016.11.054.

References

[1] M.A.A. Aziz, A.A. Jalil, S. Triwahyono, A. Ahmad, Green Chem. 17 (2015) 2647–2663.
[2] T. Sakakura, J.C. Choi, H. Yasuda, Chem. Rev. 107 (2007) 2365–2387.
[3] R.L. Paddock, S.B.T. Nguyen, JACS 123 (2001) 11498–11499.
[4] D. Day, R.J. Evans, J.W. Lee, D. Reicosky, Energy 30 (2005) 2558–2579.
[5] K.A. Pokrovski, A.T. Bell, J. Catal. 244 (2006) 43–51.
[6] W.L. Dai, S.L. Luo, S.F. Yin, C.T. Au, Appl. Catal. A 366 (2009) 2–12.
[7] T. Iijima, T. Yamaguchi, Appl. Catal. A 345 (2008) 12–17.
[8] Q. Zhang, Y.Z. Zuo, M.H. Han, J.F. Wang, Y. Jin, F. Wei, Catal. Today 150 (2010) 55–60.
[9] T. Inui, T. Takeguchi, Catal. Today 10 (1991) 95–106.
[10] J. Gao, Q. Liu, F. Gu, B. Liu, Z. Zhong, F. Su, RSC Adv. 5 (2015) 22759–22776.
[11] J. Sehested, Catal. Today 111 (2006) 103–110.
[12] H.H. Gierlich, M. Fremery, A. Skov, J.R. Rostrup-nielsen, Stud. Surf. Sci. Catal. 6 (1980) 459–469.
[13] G. Du, S. Lim, Y. Yang, C. Wang, L. Pfefferle, G.L. Haller, J. Catal. 249 (2007) 370–379.

[14] N. Yao, H. Ma, Y. Shao, C. Yuan, D. Lv, X. Li, J. Mater. Chem. 21 (2011) 17403–17412.
[15] S. Eckle, Y. Denkwitz, R.J. Behm, J. Catal. 269 (2010) 255–268.
[16] C. Janke, M.S. Duyar, M. Hoskins, R. Farrauto, Appl. Catal. B 152 (2014) 184–191.
[17] I. Czekaj, F. Loviat, F. Raimondi, J. Wambach, S. Biollaz, A. Wokaun, Appl. Catal. A 329 (2007) 68–78.
[18] J.R. Rostrup-Nielsen, K. Pedersen, J. Sehested, Appl. Catal. A 330 (2007) 134–138.
[19] T.T.M. Nguyen, L. Wissing, M.S. Skjeth-Rasmussen, Catal. Today 215 (2013) 233–238.
[20] G.D. Weatherbee, C.H. Bartholomew, J. Catal. 77 (1982) 460–472.
[21] D.E. Peebles, D.W. Goodman, J.M. White, J. Phys. Chem. 87 (1983) 4378–4387.
[22] M. Marwood, R. Doepper, A. Renken, Appl. Catal. A 151 (1997) 223–246.
[23] A.L. Lapidus, N.A. Gaidai, N.V. Nekrasov, L.A. Tishkova, Yu A. Agafonov, T.N. Myshenkova, Pet. Chem. 47 (2007) 75–82.
[24] K.J. Williams, A.B. Boffa, M. Salmeron, A.T. Bell, G.A. Somorijai, Catal. Lett. 9 (1991) 415–426.
[25] Y. Men, G. Kolb, R. Zapf, V. Hessel, H. Lowe, Catal. Today 125 (2007) 81–87.
[26] M. Kramer, M. Duisberg, K. Stowe, W.F. Maier, J. Catal. 251 (2007) 410–422.
[27] R.A. Dagle, Y. Wang, G.G. Xia, J.J. Strohm, J. Holladay, D.R. Palo, Appl. Catal. A 326 (2007) 213–218.
[28] Z.G. Zhang, G. Xu, Catal. Commun. 8 (2007) 1953–1956.
[29] L. Fan, N. Ichikuni, S. Shimazu, U. Takayoshi, Appl. Catal. A 246 (2003) 87–95.
[30] H. Hakkinen, U. Landman, J. Am. Chem. Soc. 123 (2001) 9704–9705.
[31] Z. Ding, H. Yang, J. Liu, W. Dai, X. Chen, X. Wang, X. Fu, Appl. Catal. B 101 (2011) 326–332.
[32] W.J. Shen, M. Okumura, Y. Matsumura, M. Haruta, Appl. Catal. A 213 (2001) 225–232.
[33] X. Lin, K. Yang, R. Si, X. Chen, W. Dai, Appl. Catal. B 147 (2014) 585–591.
[34] S. Wang, G.Q.M. Lu, Appl. Catal. B 19 (3) (1998) 267–277.
[35] G. Yang, Z. Jiang, H. Shi, T. Xiao, Z. Yan, J. Mater. Chem. 20 (2010) 5301–5309.
[36] A. Kudo, K. Omori, H. Kato, J. Am. Chem. Soc. 121 (1999) 11459–11467.
[37] Z. Jiang, F. Yang, N. Luo, B.T.T. Chu, D. Sun, H. Shi, T. Xiao, P. Edwards, Chem. Commun. 47 (2008) 6372–6374.
[38] X. Chen, X. Wang, Y. Hou, J. Huang, L. Wu, X. Fu, J. Catal. 255 (2008) 59–67.
[39] S.N. Frank, A.J. Bard, J. Am. Chem. Soc. 99 (1977) 303–304.
[40] D.F. Ollis, E. Pelizzetti, N. Sperone, Photocatalysis: Fundamentals and Applications, John Wiley, New York, 1989, pp. 603–636.
[41] Y. Bai, W. Li, C. Liu, Z. Yang, X. Feng, X. Lu, K. Chan, J. Mater. Chem. 19 (2009) 7055–7061.
[42] Z. Zhang, J. Long, X. Xie, H. Lin, Y. Zhou, R. Yuan, W. Dai, Z. Ding, X. Wang, X. Fu, ChemPhysChem 13 (2012) 1542–1550.
[43] C.D. Valentin, G. Pacchioni, A. Selloni, S. Livraghi, E. Giamello, J. Phys. Chem. B 109 (2005) 11414–11419.
[44] J. Premkumar, R. Ramaraj, J. Mol. Catal. A: Chem. 142 (1999) 153–162.
[45] T. Wu, G. Liu, J. Zhao, H. Hidaka, N. Serpone, J. Phys. Chem. B 102 (1998) 5845–5851.
[46] D.C. Upham, A.R. Derk, S. Sharma, H. Metiu, E.W. Mcfarland, Catal. Sci. Technol. 5 (2015) 1783–1791.
[47] D. Panayotov, J.T. Yates Jr., Chem. Phys. Lett. 381 (2003) 154–162.
[48] X. Wang, Y. Li, X. Liu, S. Gao, B. Huang, Y. Dai, Chin. J. Catal. 36 (2015) 389–399.
[49] L. Zhang, J.M. Mou, Nanomaterials and Nanostructure, Science Press, Beijing, 2001, pp. 312.
[50] A. Karelovic, P. Ruiz, Appl. Catal. B 113 (2012) 237–249.
[51] I. Nakamura, H. Nakano, T. Fujitani, T. Uchijima, J. Nakamura, Surf. Sci. 402 (1998) 92–95.
[52] I. Tankov, W.H. Cassinelli, J.M.C. Bueno, K. Arishtirova, S. Damyanova, Appl. Surf. Sci. 259 (2012) 831–839.
[53] Z.M. El-Bahy, Mod. Res. Catal. 2 (2013) 136–147.
[54] K. Hadjiivanov, J. Lamotte, J.C. Lavalley, Langmuir 13 (1997) 3374–3381.
[55] R.A. Niquist, R.O. Kagel, Infrared Spectra of Inorganic Compounds, Academic Press, New York, 1971, pp. 1–18.
[56] J.C. Elliott, Structure and Chemistry of the Apatites and Other Calcium Orthophosphates, Elsevier, 2013.
[57] M. Marwood, R. Doepper, A. Renken, Appl. Catal. A 151 (1997) 223–246.
[58] C. Crisafulli, R. Maggiore, S. Scire, S. Galvagno, J. Chem. Soc. Faraday Trans. 90 (1994) 2809–2813.
[59] G.H. Yokomizo, C. Louis, A.T. Bell, J. Catal. 120 (1989) 1–14.
[60] C. Crisafulli, S. Scire, R. Maggiore, S. Minico, S. Galvagno, Catal. Lett. 59 (1999) 21–26.
[61] J. Tang, Y. Wang, A. Deng, H. Yuan, K. Zhou, Chin. J. Nonferrous Met. 17 (2007) 1555–1560.
[62] M. Toth, J. Kiss, A. Oszko, G. Potari, B. Laszlo, A. Erdohelyi, Top. Catal. 55 (2012) 747–756.
[63] S. Neatu, J.A. Macia-Agullo, P. Concepcion, H. Garcia, J. Am. Chem. Soc. 136 (2014) 15969–15976.
[64] R. Si, J. Liu, Y. Zhang, X. Chen, W. Dai, X. Fu, Appl. Surf. Sci. 387 (2016) 1062–1071.
[65] H. Ishikawa, J.N. Kondo, K. Domen, J. Phys. Chem. B 103 (1999) 3229–3234.
[66] H. Tang, K. Prasad, R. Sanjines, F. Levy, Sens. Actuators B 26 (1995) 71–75.
[67] T. Iwanaga, T. Hyodo, Y. Shimizu, M. Egashira, Sens. Actuators B 93 (2003) 519–525.
[68] M.A.A. Aziz, A.A. Jalil, S. Triwahyono, R.R. Mukti, Y.H. Taufiq-Yap, M.R. Sazegar, Appl. Catal. B 147 (2014) 359–368.
[69] W. Dai, X. Chen, X. Zheng, Z. Ding, X. Wang, P. Liu, X. Fu, ChemPhysChem 10 (2009) 411–419.
[70] G.B. Raupp, J.A. Dumesic, J. Phys. Chem. 89 (1985) 5240–5246.
[71] I.Z. Bunin, V.A. Chanturiya, M.V. Ryazantseva, N.E. Anashkina, E.V. Koporulina, Bull. Russ. Acad. Sci. Phys. 80 (2016) 645–649.
[72] W. Dai, X. Wang, P. Liu, Y. Xu, G. Li, X. Fu, J. Phys. Chem. B 110 (2006) 13470–13476.
[73] Z. Zhang, X. Wang, J. Long, Q. Gu, Z. Ding, X. Fu, J. Catal. 276 (2010) 201–214.
[74] H. Wang, X. Yang, W. Xiong, Z. Zhang, Res. Chem. Intermed. 41 (2015) 3981–3997.
[75] Z. Zheng, J. Teo, X. Chen, H. Liu, Y. Yuan, E. Waclawik, Z. Zhong, H. Zhu, Chem. Eur. J. 16 (2010) 1202–1211.
[76] Y. Xie, Q. Zhao, X.J. Zhao, Y. Li, Catal. Lett. 118 (2007) 231–237.
[77] W. Gopel, J. Anderson, D. Frankel, M. Jaehnig, K. Philips, J. Schafer, G. Rocker, Surf. Sci. 139 (1984) 333–346.
[78] D. Chandra, N.K. Mal, M. Mukherjee, A. Bhaumik, J. Solid State Chem. 179 (2006) 1802–1807.
[79] L. Jing, X. Sun, B. Xin, B. Wang, W. Cai, H. Fu, J. Solid State Chem. 177 (2004) 3375–3382.
[80] Z.H. Cheng, A. Yasukawa, K. Kandori, T. Ishikawa, Langmuir 14 (1998) 6681–6686.
[81] H. Wu, J.M. Simmons, G. Srinivas, W. Zhou, T. Yildirim, J. Phys. Chem. Lett. 1 (2010) 1946–1951.